published by Ural Federal University
eISSN 2411-1414
chimicatechnoacta.ru

REVIEW
2025, vol. 12(2), No. 12207
DOI: 10.15826/chimtech.2025.12.2.07

Manganese- and bismuth-containing phosphors based on $MMeBO_3$ (M = Li, Na, K; Me = Mg, Ca, Sr, Ba, Zn) for white LEDs

Tatyana Khamaganova *, Alexandra Logvinova

Baikal Institute of Nature Management of the Siberian Branch of the Russian Academy of sciences, Ulan-Ude, 670047, Russia
* Corresponding author: khama@binm.ru

Abstract

White light-emitting diodes (LEDs) are a new generation of light sources that are used in solid-state lighting and information display devices. They generate less thermal radiation than incandescent and fluorescent lamps. Phosphor light-emiting diodes (PC-LEDs), which are based on this technology, have high luminous efficiency and energy efficiency; they are compact and havy a long service life. LED materials are subject to such requirements asenvironmental friendliness, transparency of the radiation source used in the excitation process, and color rendering efficiency. For use in LEDs, it is necessary to investigate optical properties of inorganic materials that are doped not only with rare earth elements (due to their high cost) but also with transition metal ions such as Mn^{2+}. This review summarizes and analyses information on the synthesis, structure, and photoluminescent properties of borates $MMeBO_3$, where M = Li, Na, K; Me = Mg, Ca, Sr, Ba, Zn doped with Mn^{2+} and Bi^{3+} and co-doped with rare earth metals (Ce^{3+}, Eu^{3+}). Impurity ions of activators, when introduced into a compound's lattice, become the main luminescent centers of phosphors. Processes of energy transfer from the sensitizer to the activator and their mechanisms are discussed. The dependence on the size and morphology of particles of the materials' luminescence efficiency is discussed. The possibility of using borates as matrices for phosphors emitting red light is shown, along with their tunable luminescence for use in white LEDs and autoemission displays.

Key findings

- Borates $NaSrBO_3$:0.01Ce^{3+},0.07Tb^{3+} and $KMgBO_3$:0.09Mn^{2+} showed high quantum efficiency values.
- Devices made on the basis of $NaCa_{0.96}BO_3$:Ce^{3+},Mn^{2+}, $NaSr_{0.89}BO_3$:Ce^{3+},Tb^{3+},Mn^{2+} can produce light close to white.
- Borates $MMeBO_3$ doped with Mn^{2+}, Bi^{3+} are very promising materials for white LEDs.

Accompanying information

Article history
Received: 14.11.24
Revised: 06.12.24
Accepted: 21.12.24
Available online: 23.01.25

Keywords
white light-emitting diodes, photoluminescence, activator, sensitizer, energy transfe, quantum efficiency

Funding
This work was supported by the Ministry of Science and Higher Education of the Russian Federation (the government order to the Baikal Institute of Nature Management, Siberian Branch of the Russian Academy of Sciences, project No.0273-2021-0008).

Supplementary information
Transparent peer review: READ

Sustainable Development Goals

1. Introduction

Interest in activated inorganic phosphors has especially increased in recent decades due to the development of a new generation of light sources [1–10]. White light-emitting diodes (Pc-WLED) have become the main source of solid-state lighting and information display devices [9–13].

The development of light sources requires continuous improvement in the performance of white LED (WLED) and multicolor 3D displays to improve energy efficiency, color rendering, luminance, lifetime, and other characteristics.

As is known, the phenomenon of luminescence occurs as a result of the electron transition emission in molecules or crystals from one energy level to another, lower energy level. The substance must be transparent to the source of radiation used in the excitation process. For luminescence to occur, it is important to have activators (impurity ions and lattice defects) occupying discrete energy levels in the forbidden zone. In insulators and conductors, the forbidden zone exists between the conduction band and the valence band. Luminescence centers are defect centers that can be intrinsic (electron-hole) centers or impurity centers [14].

According to their electronic structure, these centers are classified into several types. The most common types are ions of rare earth elements and transition metal ions. The vast majority of commercially available PC-wLEDs are made from a blue LED and phosphors that photoluminesce to convert the wavelength. Some of the blue photons emitted by the chip are absorbed by phosphors and converted to lower-energy photons spectrally. The combination of these blue photons with photons converted at decreasing frequencies results in white light [4–7, 11–15]. Currently, the most popular phosphors on the market are made from materials containing rare earth elements in their composition. But due to the high cost and complexity of producing the latter, there is an urgent need for reliable substitutes for REE in photonic devices.

Current commercial white light-emitting diode (w-LED) devices use a yellow phosphor $Y_3Al_5O_{12}:Ce^{3+}$ (YAG:Ce) with a blue chip (InGaN). This device has disadvantages such as low color rendering index (CRI, R_a < 75) and a high correlated color temperature (CCT) due to the lack of red light [16, 17]. Therefore, stable red phosphors with good luminescent properties are in great demand. In red phosphors based on inorganic compounds, trivalent REEs such as Eu^{3+}, Pr^{3+}, Sm^{3+}, and Eu^{2+} are used as luminescent centers [18–21].

The occurrence of luminescence is associated with three elementary processes: excitation (absorption), emission of light and non-radiative transitions. Due to the interaction of the activator ion with the surrounding crystal field, part of the excitation energy is transferred to the crystal lattice, which leads to a Stokes shift of the emission band relative to the corresponding absorption band towards longer wavelengths. The stronger the interaction between the activator and the lattice, the larger the Stokes shift and the wider the emission [14].

For use in LEDs, the optical properties of materials doped with not only REEs but also transition metal ions such as Cr^{3+} [22–24] and Mn^{2+} [25–28] are widely studied. The Mn ions act as activators and exhibit different valence states in different phosphors. The most common are divalent Mn^{2+} and tetravalent Mn^{4+}. Typically, the Mn^{2+} ion exhibits broad emission from green to dark red due to the electronic transition $^4T_1(^4G) \rightarrow {}^6A_1(^6S)$, in which the excitation level $^4T_1(^4G)$ decreases with increasing crystal field, causing the red shift in emission. The color of radiation depends on the strength of the crystal field of the basic lattice and the coordination number of Mn^{2+} ions. Green radiation is produced by an Mn^{2+} ion in a weak crystal field coordinated tetrahedrally [30, 31]. In materials with strong crystal fields and octahedral environments, the Mn^{2+} ion shows orange to dark-red emission [26, 32–34].

Along with the selection of a suitable activator, the choice of the carrier matrix plays an important role in creating effective phosphors. The matrix should be a chemically and thermally stable compound that does not undergo any changes under conditions of long-term use at elevated temperatures. At the same time, the carrier material must be optically transparent to the emitted light. In the absence of energy transfer from the carrier lattice to the activator, the matrix material also must be transparent to the pump LED radiation [4].

Borate compounds are promising as matrices for phosphors due to their excellent physical and chemical properties, including wide transparency region, high thermal stability, wide band gap, high quantum efficiency, and strong absorption in the ultraviolet (UV) region [15, 20–22, 28, 32].

This paper systematizes information on the synthesis, structures and luminescent properties of borate materials $MMeBO_3$, where M = Li, Na or K; Me = Mg, Ca, Sr, Ba, Zn, Cd, doped with divalent Mn^{2+} ions, as well as heavy metal ions Bi^{3+}, Pb^{2+}, co-doped with REE (Ce^{3+}, Eu^{3+}, Eu^{2+}).

2. Solid-phase synthesis of borates $MMeBO_3$, M = Li, Na, K; Me = Mg, Ca, Sr, Ba, Cd, Zn

This method uses direct interaction of mixtures of initial reagents during heating; therefore, the key role is played by the initial substances, the physical and chemical properties of which determine the choice of processing parameters.

The main parameters of the calcination process are the heating rate, duration and temperature of annealing, and atmosphere. The rate of solid-phase reaction depends on the surface area of the reagents, the diffusion rate of the initial ions and reaction products, and the rate of nucleation of a new phase.

The use of the solid-phase reaction method makes it possible to obtain particles with a high degree of crystallinity and large sizes (usually particles with sizes of 3–5 μm are obtained) [4, 35]. For LED and display applications, particle size and their distribution are essential. For example, a material with a high external quantum efficiency allows the use of less material in the manufacture of an LED chip. Activators with high absorption coefficient ($Eu^{2+}$and Ce^{3+}) are more promising than REE ions with linear emission and low absorption strength for 4f–4f transitions. In a coarse-grained phosphor material, absorption losses increase due to scattering of the converted light, which reduces the total number of photons extracted from the phosphor layer. Consequently, the scattering losses will be determined by the particle size and distribution. These parameters are important in the manufacture of lighting devices, since a wide particle size distribution can lead to inhomogeneous emission colors [8]. The need to control the particle size and distribution in the LED package was reported [4]. Thus, the uniform size distribution of red, green and blue luminescence avoids cascade excitation and thereby increases the luminescence efficiency.

 DOI: 10.15826/chimtech.2025.12.2.07

The influence of different crystallite sizes in $Y_2O_3:Eu^{3+}$ and $LaPO_4:Ce^{3+}$ phosphors on the photoluminescence emission intensities was studied in [36]. The authors used solid-phase synthesis method, combustion and co-precipitation reactions, hydrothermal, sol-gel, and spray pyrolysis. The powders of both compositions showed almost similar crystallite sizes obtained by spray pyrolysis, hydrothermal, co-precipitation and solid-phase methods. The PL emission intensity increased with increasing crystallite size, but no precise correlation was found between the PL emission intensity and particle size. The traditional method of solid-phase synthesis has been used to obtain $MMeBO_3$ borates doped with Mn^{2+} ions [28, 37, 38] and co-doped Ce^{3+}/Mn^{2+} [40, 41, 43–45], Eu^{3+}/ Bi^{3+} [39, 42], Eu^{3+}/ Mn^{2+} [46] ions presented in this review. Table 1 presents the conditions for the solid-phase synthesis of the studied materials.

Table 1 shows that the solid-phase synthesis of $MMeBO_3$ is carried out, as a rule, by two-stage annealing of the starting substances, less often – by three-stage or one-stage annealing. The initial components are carbonates of the corresponding metals and boric acid, which is taken in a small excess, taking into account the losses due to sublimation. The annealing is carried out in a reducing atmosphere to prevent oxidation processes.

3. Crystal structure of $MMeBO_3$

Crystal structures and luminescent properties of $LiMeBO_3$, Me = Mg, Ca, Sr, Ba, Zn, Cd were described earlier [47]. In the present work, we will focus on the structures of sodium and potassium orthoborates with this composition in more detail.

The data on the crystal structure of $MMeBO_3$ borates are presented in Table 2. It can be seen that the coordination in the presented structures changes according to the sizes of alkali and alkaline-earth metal cations.

All known orthoborates of the composition $MMeBO_3$, despite sharing the same formula, differ in structure: most of them belong to the monoclinic syngony, but $LiCaBO_3$ and $NaCaBO_3$ belong to the rhombic system (Table 2). The planar BO_3-groups are distributed differently in these compounds. They are almost parallel to each other in $LiMgBO_3$ and perpendicular in $LiCaBO_3$, while in other compounds they are distributed parallel along different directions. The structures differ in the type of coordination of the alkali and alkaline earth metals. Li atoms with a coordination number (CN = 5) form distorted trigonal bipyramides. Mg cations coordinated by 5 O atoms in $LiMgBO_3$ form trigonal bipyramides. Figure 1 shows the structural transformation from $K/RbMgBO_3$ to $Li/NaMgBO_3$ [59].

The Na atoms in $NaSrBO_3$ and $NaBaBO_3$ have one coordination (CN = 6), forming octahedra. The Sr and Ca atoms have CN = 7 in $LiSrBO_3$ and $LiCaBO_3$, the Sr and Ba atoms have CN = 9 in $NaSrBO_3$ and $NaBaBO_3$, similar to the environment of the Ba atoms in $LiBaBO_3$.

The Ca atoms are surrounded by 7 O atoms, forming single-cap trigonal prisms in $LiCaBO_3$. In contrast to the structures of lithium borates of $LiMeBO_3$, a mixed occupancy of the positions of Ca atoms with Na atoms was found in the structure of $NaCaBO_3$ (partial substitution by 20% Na) [53]. In the structure of $NaCaBO_3$, two mixed positions M1 and M2 were found, differing in the oxygen environment: M1 has a CN = 7, and M2 has a CN = 6. In addition, 2 independent Na atoms with an oxygen environment of 8 and 6 atoms isolated; their polyhedra, connecting by edges and faces, form chains along the *c* axis.

Table 1 Conditions for solid-phase synthesis of borates doped with Mn^{2+} and Bi^{3+} and co-doped with Ce^{3+} and Eu^{3+}.

Material	Starting substances	Restore atmosphere	Annealing mode	Particle sizes (μm)	Ref.
$LiMgBO_3:Mn^{2+}$	Li_2CO_3, MgO, Na_2CO_3, K_2CO_3, $MnCO_3$, H_3BO_3	15% H_2/85% Ar	600 °C (24 h), 800 °C (48 h), 800 °C (6 h)	12	37
α-$LiZnBO_3:Mn^{2+}$	Li_2CO_3,ZnO, $MnCO_3$, H_3BO_3	15% H_2/85% Ar	500 °C (24 h), 900 °C (6 h)	8–18	38
$KMgBO_3:Mn^{2+}$	K_2CO_3, MgO, $MnCO_3$, H_3BO_3	5% H_2/95% Ar	550 °C (24 h), 800 °C (8 h)	–	28
$LiMgBO_3:Eu^{3+}/Bi^{3+}$	Li_2CO_3,MgO, Eu_2O_3, Bi_2O_3, H_3BO_3	–	700–800 °C (8 h)	3–5	39
$LiCaBO_3:Ce^{3+}/Mn^{2+}$	$CaCO_3$, CeO_2, $MnCO_3$, H_3BO_3 Li_2CO_3 excess	C for recovery Ce^{4+}до Ce^{3+}	500 °C (3 h), 750 °C (6 h)	–	40
$LiBaBO_3:Ce^{3+}/Mn^{2+}$	Li_2CO_3,$BaCO_3$, CeO_2, $MnCO_3$, 3 % mol. H_3BO_3	95% H_2/5% N_2	400 °C (3 h), 800 °C (4 h)	–	41
$LiBaBO_3:Eu^{3+}/Bi^{3+}$	Li_2CO_3,$BaCO_3$, Eu_2O_3, Bi_2O_3, H_3BO_3	–	800 °C (5 h)	43, 29 (nm) 58, 28 (nm)	42
$NaMgBO_3:Ce^{3+}/Mn^{2+}$	$NaHCO_3$, CeO_2, $MgCO_3$, $MnCO_3$, 3 % mol. H_3BO_3	5% H_2/95% N_2	< 650 °C (7 h), 650 °C (8 h), 750 °C	–	43
$NaCaBO_3:Ce^{3+}/Mn^{2+}$	Na_2CO_3,$CaCO_3$,CeO_2, $MnCO_3$, H_3BO_3	5% H_2/95% N_2	900 °C (8 h)	–	44
$NaSrBO_3:Ce^{3+}/Mn^{2+}$	Na_2CO_3, $SrCO_3$, CeO_2, $MnCO_3$, 5 % mol. H_3BO_3	5% H_2/95% N_2	850 °C (8 h)	–	45
$NaCaBO_3:Eu^{3+}/Mn^{2+}$	Na_2CO_3,$CaCO_3$, $MnCO_3$, Eu_2O_3, 3 % mol. H_3BO_3	5% H_2/95% N_2	400 °C (1 h), 850 °C (3 h)	–	46

 DOI: 10.15826/chimtech.2025.12.2.07

Table 2 Coordination numbers of cations in $MMeBO_3$ structures.

Material	Crystal system	Sp. gr.	CN (M)	CN (Me)	CN (B)	Ref.
$LiMgBO_3$	monocl.	C2/c	5	5	3	48
$LiCaBO_3$	rhomb.	Pbca	5	7	3	49
$LiSrBO_3$	monocl.	$P2_1/n$	5	7	3	50
$LiBaBO_3$	monocl.	$P2_1/n$	5	9	3	50
α-$LiZnBO_3$	monocl.	C2/c	5	4	3	51
$NaMgBO_3$	monocl.	C2/c	8	6	3	52
$NaCaBO_3$	rhomb.	Pmmn	6,8	6,7	3	53
$NaSrBO_3$	monocl.	$P2_1/c$	6	9	3	54
$NaBaBO_3$	monocl.	C2/m	6	9	3	55, 56
$KMgBO_3$	cubic.	$P2_13$	6	6	3	57
$KCaBO_3$	monocl.	$P2_1/c$	5	7	3	58

The main structural elements are isolated BO_3-anionic groups distributed parallel to four directions, namely [301], [$\bar{3}$01], [032], [0$\bar{3}$2].

In none of the $LiMeBO_3$ borates was a joint occupation of positions by cations detected. The authors of [53] attribute this to the large difference in the sizes of Li^+ and divalent cations. The coordination numbers in the structures of $MMeBO_3$ according to data from different authors are given in Table 2.

A close relationship was found between the structures of $NaMgBO_3$ and $NaSrBO_3$, which manifests itself in the exchange of positions of the alkali and alkaline earth metal ions [52]. Thus, Mg atoms in $NaMgBO_3$ occupy the positions of Na atoms in the structure of $NaSrBO_3$, and Na atoms occupy the positions of Sr atoms. The difference in the valences of the substituting metals leads to a significant deformation of the $NaMgBO_3$ structure, leading to an increase in its symmetry (see Table 2). The diversity of crystal structures can be explained by the significant activity of alkali and alkaline earth metals.

4. Doping of $MMeBO_3$ with Mn^{2+} and Bi^{3+} ions

Rare earth elements (REE) used in phosphors are usually expensive, and most phosphors require high synthesis temperatures and harsh preparation conditions [26–28]. All this limits their wide application; therefore, great efforts are being made to create materials that do not contain REE ions, with low cost and mild production conditions, for use in LEDs [26, 28]. Alternative materials with good luminescent properties are phosphors doped with Mn^{2+}. They are capable of providing high luminescence efficiency and color purity when excited by a wide variety of excitation methods (UV light, electron beams, etc.).

The Mn^{2+} ion has a d^5 electronic configuration and is widely used in inorganic phosphors as a red light activator. The emission of the ion occurs due to the parity forbidden dipole-dipole (d–d- transitions) $^4T_1$ and $^6A_1$ [12, 17, 32, 41, 60]. Depending on the strength and the crystalline field of the matrix, the color of the Mn^{2+} emission can vary from green to dark red.

Some borates such as β-$Zn_3B_2O_6$:Mn^{2+} [32], $LiMgBO_3$:Mn^{2+} [37], $KMgBO_3$:Mn^{2+} [28], ZnB_2O_4:Mn^{2+} [61] were shown to be promising luminescent matrices for LEDs.

Mn^{2+} and heavy metal (Bi^{3+}, Pb^{2+}) ions are doped together with rare earth ions [43–46, 60, 62–65] to enhance the emission intensity and color tuning. For example, Ce^{3+} acts as a good sensitizer by transferring part of its energy to the activator ion. By co-doping an inorganic matrix with Ce^{3+} and Mn^{2+} ions with effective resonance-type energy transfer, white light can be obtained.

As is known, the condition for resonant energy transfer is the overlap between the emission spectrum of the sensitizer and the absorption spectrum of the activator. It can be realized through exchange interaction and electrical multipolar interaction [66].

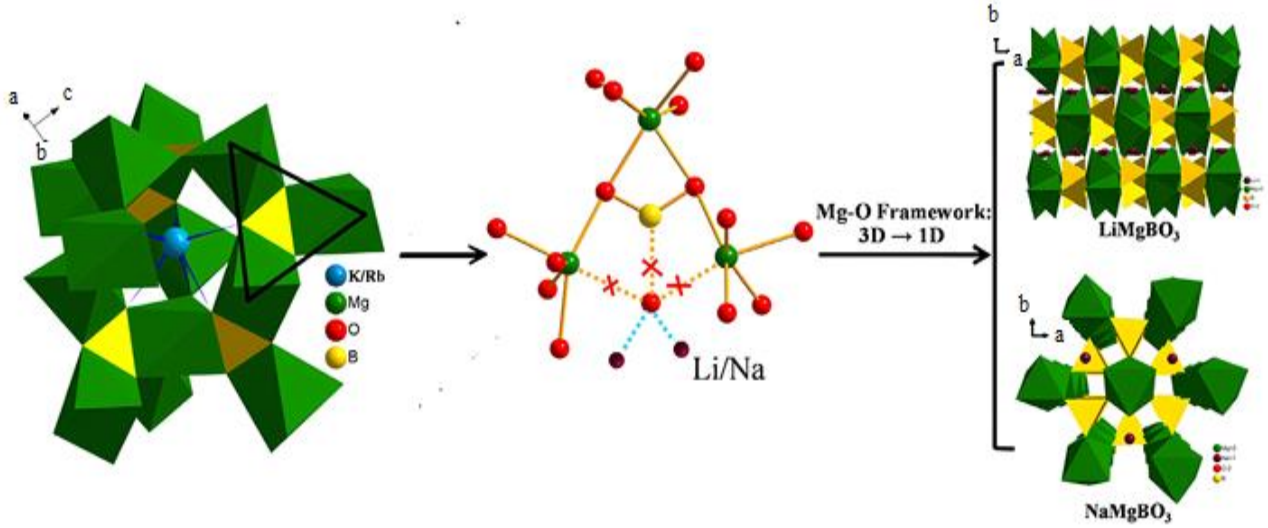

Figure 1 Structural transformation from K/$RbMgBO_3$ to Li/$NaMgBO_3$ (green tetrahedra are MgO_4, yellow triangles are BO_3) [59].

 DOI: 10.15826/chimtech.2025.12.2.07

The emission of the Bi^{3+} ion as an activator is associated with the transition of electrons between the ground state $6s^2$ and the excited states 6s6p. It exhibits strong interaction with the lattice and energy transfer from one Bi^{3+} ion to another Bi^{3+} ion or to another activator. The optical properties of Bi^{3+} ions with the external electron configuration $6s^2$ depend on a number of conditions, such as covalence, coordination number and symmetry of the sites. Therefore, depending on the matrix, the luminescence of Bi^{3+} ions can vary from the ultraviolet to the red region of the spectrum [67–69]. Bi^{3+} ions, being a co-activator, can become a sensitizer, acting as a primary excitation energy center and nonradiatively transferring their energy to enhance the radiation intensity of another dopant ion [69].

5. Relationship between structure and luminescent properties

Wu et al. [37] refined the structure of $LiMgBO_3$:0.04Mn^{2+} by the Rietveld method. It turned out that Mn^{2+} ions statistically fill two crystallographically independent positions of Li ions with a coordination number of 5. Their polyhedra are described as strongly distorted trigonal bipyramids. The significant distortion of trigonal bipyramides is due to the partial filling of both Li^+ positions with activator ions. This leads to further splitting of the E and T levels of Mn^{2+} ions and shifts the first excited state $^4T_1$ (^4G) towards lower energy. The structure model was confirmed by measuring the electron paramagnetic resonance (EPR) spectra of the two samples. The presence of two emission centers in the emission spectrum of the $LiMgBO_3$:0.04Mn^{2+} sample indicates the presence of two different positions of the activator ions in the main lattice.

From the analysis of the factors characterizing the strong crystal field (activator charge, Mn - O distances), it can be seen that the reason for the dark red emission band is the splitting of the d-levels of the Mn^{2+} ion. The crystal structure of α-$LiZnBO_3$ consists of ZnO_4 tetrahedra connected by vertices, BO_3 triangles and Li pentahedra [38]. Each Zn atom has a distorted tetrahedral coordination, and two ZnO_4 tetrahedra with an inversion center, connecting by a common edge, form a Zn_2O_6 dimer. X-ray diffraction confirmed that the α-$LiZnBO_3$ matrix doped with Mn^{2+} ions crystallizes in a monoclinic lattice, space group C2/c, with parameters a = 8.746 (2), b = 5.091 (1), c = 6.129 (1) Å, β = 118.75 (3) ° [38]. The authors' assumptions about the placement of Mn^{2+} ions in the positions of Zn^{2+} ions were confirmed by the research results. The unalloyed sample showed white daylight due to strong reflection in the visible area.

The EPR spectra of undoped and doped α-$LiZnBO_3$ samples were characterized by strong resonance peaks indicating the contribution of the Mn^{2+} ion spin. The absorption in the region below 220 nm was attributed to the ultraviolet absorption of the matrix according to the diffuse reflectance spectra. The peak at 238 nm is attributed to the charge transfer state (CTS) $O^{2-} \rightarrow Mn^{2+}$. The absorption in the 300–600 nm region is mainly due to the d–d transition of Mn^{2+}, and the intense absorption band can be explained by the transition from the ground state $^6A_1$ to the excited state $^4T_1$ of the Mn^{2+} ion. Manganese-doped α-$LiZnBO_3$ samples show white or pale pink color with increasing Mn^{2+} concentration. All transitions from the excited d5 level are spin forbidden, so the optical absorption of Mn^{2+} is usually weak, as, for example, in Zn_2SiO_4 [70].

The strong absorption band in α-$LiZnBO_3$:Mn^{2+} indicates obvious deviations from the selection rules. Figure 2 shows the crystal structure of $NaMgBO_3$:Ce^{3+},Mn^{2+} and the coordination environment of metal cations according to [43]. The ions introduced jointly into the monoclinic structure replace the Na^+ and Mg^{2+} ions according to their sizes. It is shown that Ce^{3+} ions partially replace the Na^+ positions, and Mn^{2+} ions substitute the Mg^{2+} positions.

6. Photoluminescent properties

6.1. Influence of morphology and particle size on luminescence

There are few works that examined the size and shape of particles, as well as the effect of co-doping on their morphology. The morphology of homogeneous $LiMg_{0.75}BO_3$:0.25Eu^{3+} crystals, which had an average particle size of about 3–5 μm, was investigated by scanning electron microscopy (SEM) [39]. According to [71, 72] the small size and uniform shape of crystals can increase their density and enhance the luminescence intensity of materials.

Based on the results of the particle size study of the original luminophore $LiMg_{0.75}BO_3$:0.25 Eu^{3+}, a change in the morphology and particle size was found upon the addition of Bi^{3+}. The particle sizes of the $LiMg_{0.945}BO_3$:0.05Eu^{3+}, 0.005Bi^{3+}phosphor increase with the introduction of a co-activator. The change in the sizes of materials doped with one and two activators according to this work can be observed in Figure 3.

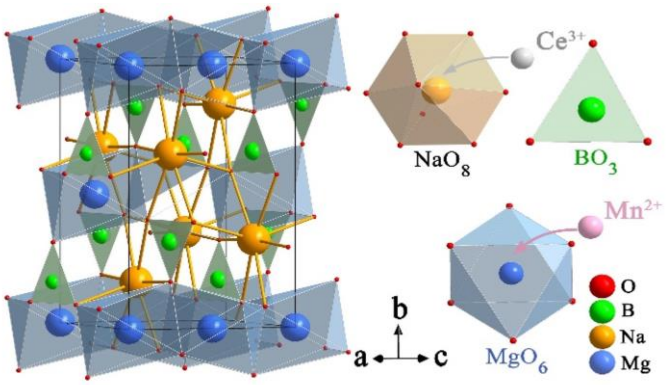

Figure 2 Crystal structure of $NaMgBO_3$:Ce^{3+},Mn^{2+} [43].

 DOI: 10.15826/chimtech.2025.12.2.07

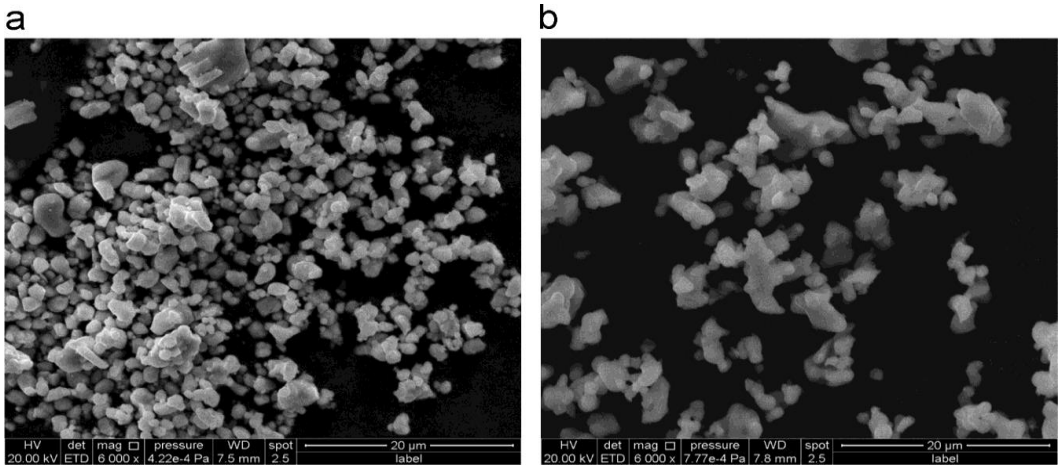

Figure 3 Images of $LiMg_{0.75}BO_3$:0.25Eu^{3+} (a) and $LiMg_{0.945}BO_3$:0.05Eu^{3+}, 0.005Bi^{3+} (b), obtained by SEM according to [39].

The excitation and emission spectra of the phosphors $LiMg_{0.75}BO_3$:0.25Eu^{3+}, $LiMg_{0.749}BO_3$:0.25Eu^{3+},0.001Bi^{3+} were investigated [39]. In the excitation spectra of both phosphors, the lines assigned to the 4f -transitions of Eu^{3+} ($^7F_0 \rightarrow {}^5D_2$ at 466 nm and $^7F_0 \rightarrow {}^5L_6$ at 395 nm) as well as a broad charge transfer (CT) band of O^{2-} - Eu^{3+} in the UV region were observed. The line intensities of the Eu^{3+} 4f -transitions were higher in the sample $LiMg_{0.749}BO_3$:$Eu^{3+}_{0.25}$,$Bi^{3+}_{0.001}$. As is known, the energy levels of REE ions are split in the crystal field created by the crystal lattice. Consequently, the splitting of the levels depends on the crystal structure of the lattice itself. According to the Laporte parity selection rule, if the REE ion occupies a centrosymmetric position, only magnetic dipole transitions are possible. If the REE ion is in a non-centrosymmetric position, both magnetic dipole and electric dipole transitions are possible [44, 73]. The dominant peak located at 615 nm in the emission spectrum of $LiMg_{0.749}BO_3$:$Eu^{3+}_{0.25}$,$Bi^{3+}_{0.001}$ is attributed to the $^5D_0 \rightarrow {}^7F_2$ electric dipole transition of Eu^{3+} ions, provided that the Eu^{3+} ions are located away from the center of symmetry in the crystal lattice [39]. Another intense peak located at 593 nm is attributed to the magnetic dipole transition $^5D_0 \rightarrow {}^7F_1$ of Eu^{3+} ions. The emission spectrum indicates the influence of co-doping on the symmetry of Eu^{3+} ions in the $LiMg_{0.75}BO_3$:0.25Eu^{3+} phosphor, since the $^5D_0 \rightarrow {}^7F_1$ transition is insensitive to the position.

The luminescence intensity reached a maximum at 615 nm at a Eu^{3+} doping concentration of 25 mol %. It decreased sharply at a Eu^{3+} doping concentration of 30 mol %. The authors explain the process of PL quenching by energy migration between Eu^{3+} ions. The critical distance of energy transfer between Eu^{3+} ions R_c, calculated by the concentration quenching method, was 16.31 Å. Since the calculated R_c value of $LiMgBO_3$:Eu^{3+} is greater than 5 Å (a typical critical distance for exchange interaction), the energy transfer process cannot be limited mainly by the exchange interaction. When the $LiMgBO_3$:Eu^{3+} sample is co-doped with a sensitizer (Bi^{3+} ions), the absorption capacity of the $^7F_0 \rightarrow L_6$ and $^7F_0 \rightarrow {}^5D_2$ transitions increases. The authors attribute the increase in luminescence intensity of the $LiMg_{0.75-y}BO_3$:0.25Eu^{3+},$y$$Bi^{3+}$ sample to the energy transfer of $Bi^{3+} \rightarrow Eu^{3+}$.

The quadrupole-quadrupole interaction is indicated as the main mechanism of energy transfer in the sample. When Li^+ ions are replaced by M = K^+, Na^+ in $Li_{1-y}M_yMgBO_3$:0.04Mn^{2+}, the luminescence intensity increases with increasing doping concentration and reaches a maximum at y = 0.06 [37]. It was found that the emission intensities of $Li_{0.94}K_{0.06}MgBO_3$:0.04Mn^{2+} and $Li_{0.94}Na_{0.06}MgBO_3$: 0.04Mn^{2+} are approximately 2 and 1.5 times higher than the emission intensity of $LiMgBO_3$:0.04Mn^{2+}. According to the SEM results, the crystallites of $Li_{0.94}K_{0.06}MgBO_3$: 0.04Mn^{2+} turned out to be larger and more spherical than $Li_{0.94}Na_{0.06}MgBO_3$ and especially $LiMgBO_3$:0.04Mn^{2+}. The average particle sizes for them are shown in Table 3. The results of this work agree with the data [71–74], in which the dependence of the FL intensity of phosphors on the crystallite size and morphology of materials was observed. The data of the cited works showed that the PL intensity increases with the growth of crystallite sizes and particle sizes, respectively. The important role of the crystallite size effect compared to the particle size effect and the favorable influence of the spherical morphology on the increase in the emission intensity were noted [72].

Table 3 Particle size, chromaticity coordinates (λ_{ex} = 427 nm) at temperatures of 25 °C and 150 °C and activation energies of the studied borates according to [37].

Composition	Particle size, µm	CIE (x,y)		E_a, эВ
		25° C	150° C	
$LiMgBO_3$:0.04Mn^{2+}	12.35	(0.715, 0.285)	(0.707, 0.293)	0.254
$Li_{0.94}$ $Na_{0.06}MgBO_3$: 0.04Mn^{2+}	28.53	(0.717, 0.283)	(0.709, 0.291)	0.256
$Li_{0.94}$ $K_{0.06}MgBO_3$: 0.04Mn^{2+}	43.25	(0.717, 0.283)	(0.709, 0.292)	0.261

 DOI: 10.15826/chimtech.2025.12.2.07

Lephoto et al. [42] studied the $Bi^{3+}\rightarrow Eu^{3+}$ energy transfer mechanism in $LiBaBO_3$. The results showed tunable emission, which is associated with simultaneous broadband emission at 593 nm and narrowband emission due to *f–d* and *f–f* transitions of Eu^{2+} and Eu^{3+}, respectively. According to the results of the study, some of the Eu^{3+} ions were reduced to Eu^{2+}. The samples showed greenish-blue (493 nm) and red (613 nm) luminescence, attributed to the emission of Eu^{2+} and Eu^{3+} ions. The red narrow-band emission at 613 nm depends on the concentration of the coactivator and is significantly enhanced after co-doping with Bi^{3+}, indicating nonradiative energy transfer $Bi^{3+} \rightarrow Eu^{3+}$. Co-doping with Bi^{3+} ions changes the color of the material from whitish to orange depending on the Bi^{3+} concentration. The CIE coordinates of $LiBaBO_3:Eu^{3+}$, Bi^{3+} are given in Table 4.

The excitation and emission spectra of $LiCaBO_3$ borate doped with different concentrations of Pb^{2+} and Bi^{3+} were studied in [75]. The optimal contents of activators maximally emitting at room temperature were determined. The $LiCaBO_3:Pb^{2+}$ sample showed an emission band at 296 nm upon excitation with a wavelength of 265 nm. For the Bi^{3+} doped sample, the emission band was observed at 378 nm under excitation with a wavelength of 304 nm. The calculated Stokes shift values for the samples were 3952 nm^{-1} for $LiCaBO_3:Pb^{2+}$ and 6440 nm^{-1} for $LiCaBO_3$: Bi^{3+}, respectively. Analysis of the photoluminescent properties of both materials showed their potential for use in fluorescent lamps.

6.2. Thermal stability of luminophores

Thermal stability is an extremely important factor for evaluating the possibility of using a phosphor, which determines the effectiveness and reliability of a practical device. This characteristic of the luminescent material shows the possibility of using it at elevated temperatures.

Temperature-dependent PL spectra ($\lambda_{exc.}$ = 427 nm) and X-ray diffraction patterns for $Li_{0.94}M_{0.06}MgBO_3:0.04Mn^{2+}$, M = Li, Na, K were studied in the temperature range of 25–200 °C [37].

Table 4 CIE coordinates and excitation wavelength in doped borates of $MMeBO_3$.

Material	$\lambda_{ex.}$ (nm)	CIE coordinates (*x*, *y*)	Color	Ref.
$LiMgBO_3:0.04Mn^{2+}$	427	(0.715, 0.285)	red	37
$LiMg_{0.75-y}BO_3:0.025Eu^{3+}$, Bi^{3+}	395, 427	–	orange-red	39
α-$LiZnBO_3:0.07Mn^{2+}$	431	(0.66, 0.34)	red	38
$LiCaBO_3:0.02Ce^{3+},0.12Mn^{2+}$	349	(0.20, 0.20)	violet	40
$LiCaBO_3:Mn^{2+}$	349	(0.47, 0.52)	orange	40
$LiBaBO_3:0.05Ce^{3+},0.02Mn^{2+}$	345	(0.358, 0.251)	white	41
$LiBa_{1-x}BO_3:0.020Eu^{3+},Bi^{3+}$	325	(0.368, 0.378)	white	42
$LiBa_{1-x}BO_3:0.025Eu^{3+},Bi^{3+}$	325	(0.376, 0.366)	white	42
$NaMgBO_3:0.01Ce^{3+},0.06Mn^{2+}$	365	–	blue (475), red (710)	43
$NaCa_{0.992}$ $BO_3:0.01Ce^{3+},0.01Mn^{2+}$	360	(0.246, 0.143)	blue	44
$NaCa_{0.992}BO_3:0.01Ce^{3+},0.03Mn^{2+}$	360	(0.335, 0.259)	white	44
$NaCa_{0.992}BO_3:0.01Ce^{3+},0.10Mn^{2+}$	360	(0.489, 0.246)	orange	44
$NaCaBO_3$: $0.05Mn^{2+}$	347	(0.605, 0.395)	red	64
$NaCaBO_3:0.01Ce^{3+},0.01Mn^{2+}$	347	(0.274, 0.177)	blue	64
$NaCaBO_3:0.01Ce^{3+},0.03Mn^{2+}$	347	(0.358, 0.247)	white	64
$NaCaBO_3:0.01Ce^{3+},0.05Mn^{2+}$	347	(0.397, 0.259)	white	64
$NaCaBO_3:0.01Ce^{3+},0.11Mn^{2+}$	347	(0.540, 0.330)	orange	64
$NaCaBO_3:0.01Ce^{3+},0.01Tb^{3+}$, $0.03Mn^{2+}$	347	(0.353, 0.265)	white	64
$NaCaBO_3:0.01Ce^{3+},0.05Tb^{3+}$, $0.03Mn^{2+}$	347	(0.344, 0.313)	white	64
$NaCaBO_3:0.01Ce^{3+},0.09Tb^{3+}$, $0.03Mn^{2+}$	347	(0.354, 0.315)	white	64
$NaCaBO_3:Eu^{2+},Mn^{2+}$	330	–	blue (477), red (602)	46
$NaCaBO_3:0.07Eu^{2+},0.01Mn^{2+}$	330	(0.287, 0.308),	white	46
$NaCaBO_3:0.07Eu^{2+},0.02Mn^{2+}$	330	(0.341, 0.321),	white	46
$NaCaBO_3:0.07Eu^{2+},0.03Mn^{2+}$	330	(0.381, 0.318),	white	46
$NaCaBO_3:0.07Eu^{2+},0.05Mn^{2+}$	330	(0.465, 0.332),	orange	46
$NaCaBO_3:0.07Eu^{2+},0.07Mn^{2+}$	330	(0.535, 0.317)	orange	46
$NaSrBO_3:0.05Mn^{2+}$	360	–	red	45
$NaSrBO_3:0.01Ce^{3+},0.05Mn^{2+}$	360	–	blue (430), red (650)	45
$NaSr_{0.89}BO_3:0.013Ce^{3+},0.073Tb^{3+}$, $0.032Mn^{2+}$	365	(0.2810, 0.2505)	white	65
$KMgBO_3:0.09Mn^{2+}$	438	(0.66, 0.33)	red	28

 DOI: 10.15826/chimtech.2025.12.2.07

It was found that the shape and positions of the Mn^{2+} emission peaks are practically independent of temperature changes. The authors attribute this to the small difference in energy between the two emission centers and the statistical filling of the Li^{+} positions by the activator ions.

High-temperature X-ray diffraction showed a shift of reflections towards small diffraction angles with increasing temperature above 150 °C. The latter indicates a slight thermal expansion of the borate lattice, which further explains the behavior of the Mn^{2+} emission peaks.

Due to the thermal quenching effect, the luminescence intensity decreases with increasing temperature. According to [37], the thermal stability of photoluminescence for $Li_{0.94}M_{0.06}MgBO_3$:0.04Mn^{2+} (M = Li, Na, K) exceeds the thermal stability of the commercial red phosphor SrS:Eu^{2+} (Figure 4). It can be seen that the CIE (*x*,*y*) chromaticity coordinates and activation energy values are almost the same for all samples. The obtained results indicate a very good thermal stability of the $Li_{0.94}M_{0.06}MgBO_3$:0.04Mn^{2+} (M = Li, Na, K) phosphors.

In [44] the PL spectra of $NaCa_{0.96}BO_3$:0.01Ce^{3+},0.03Mn^{2+} were studied upon excitation at 360 nm, taken with an increase in temperature from 293 to 493 K. All spectra consist of two characteristic emission bands in the range of 365–380 nm, which are explained by the $5d^1$ – $4f^1$ transitions of Ce^{3+} ions and $^4T_1(^4G)$ – $^6A_1(^6S)$ transitions of Mn^{2+} ions in the $NaCaBO_3$ lattice. With an increase in temperature from 293 K to 493 K, the photoluminescence intensities of Ce^{3+} and Mn^{2+} ions decrease to 33.4% and 42.4%, respectively. The authors explain the thermal quenching of luminescence by the temperature dependence of the electron-phonon interaction in the luminescence center and thermally activated photoionization of the lanthanide. Both mechanisms depend on the crystal lattice of the matrix and crystallinity of the phosphors. The activation energy of electrons excited from the ground state level 4f to the $5d^1$ level of field splitting of Ce^{3+} ions was 0.26 *e*V. In addition, the thermal quenching temperature, defined as the temperature at which the PL intensity is 50% of the initial value, is about 465 K. The authors note that the $NaCa_{0.96}BO_3$:0.01Ce^{3+},0.03Mn^{2+} phosphor has better thermal stability compared to previously reported phosphors. Based on the temperature-dependent PL spectra of $NaMgBO_3$:0.01Ce^{3+},0.06Mn^{2+} at excitation of 375 nm, a tendency to change the normalized peak and integral intensities was established [43]. The emission of the $NaMgBO_3$:0.01Ce^{3+},0.06Mn^{2+} phosphor presents a thermostable luminescence of Ce^{3+} and an almost linear thermal quenching curve of Mn^{2+}. The calculated value of the maximum relative temperature sensitivity at 473 K was 0.69 % K, and the temperature resolution reached 0.01 K. The obtained data indicate the possibility of using $NaMgBO_3$:Ce^{3+},Mn^{2+} borate as the main material of sensitive temperature measurement devices with high resolution.

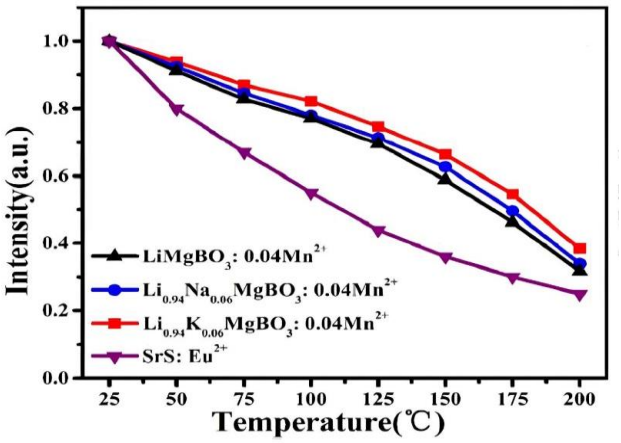

Figure 4 The temperature dependence of the photoluminescence intensity for $Li_{0.94}Mg_{0.06}BO_3$:0.04Mn^{2+} (M = Li, Na, K) compared to commercial SrS:Eu^{2+} phosphors [37].

6.3. Red phosphors

According to the existing concepts, tetrahedrally coordinated Mn^{2+} with a weak crystal field usually gives green emission. Table 5 shows the emission bans data of several representatives of different classes of compounds doped with Mn^{2+} ions. The compounds have different symmetries and crystallize in different structural types. In these compounds, the Mn^{2+} ion is tetrahedrally coordinated, but they all emit red light. The red emission observed for tetrahedrally coordinated Mn^{2+} in MZnOS compounds is explained by further splitting of the two levels of the Mn^{2+} ion into more levels in the distorted tetrahedron, leading to a shift of the first excited state towards a lower energy [76]. As a consequence, the first excited state of the Mn^{2+} ion will be located at a relatively lower energy in BaZnOS compared to CaZnOS. Therefore, longer wavelength emission for Mn^{2+} is observed in BaZnOS (634 nm) than in CaZnOS (614 nm). Due to the energy transfer between the lattice and the activator, MZnOS can be effectively excited by excitation of the matrix lattice in the wavelength range of 230–350 nm. It is shown that CaZnOS can be efficiently excited by the excitation of the Mn^{2+} ion itself in the range of 350–500 nm, which is rare for most Mn^{2+}-doped phosphors.

The special behavior is explained by the lifting of the spin and parity ban on the d–d transitions of Mn^{2+} [76]. The high absorption and strong excitation bands of $CaZn_{1-x}Mn_xOS$ in the range of 350–500 nm correspond to the emitting light of UV-blue LEDs, indicating their unique properties as conversion phosphors.

The positions of the emission bands of the studied borates $MMeBO_3$ are in the red region of the spectrum, the full width at half-height of the emission peak for α-$LiZnBO_3$:Mn^{2+} was 80 nm, and for $KMgBO_3$:Mn^{2+} it is 70 nm. These values are averages for the emission bands excited by near-UV light and fit well into the general picture (Table 5). All investigated borates emit red light, which can be traced by the corresponding chromaticity coordinates. For two representatives α-$LiZnBO_3$:Mn^{2+} and $KMgBO_3$:Mn^{2+}, the

 DOI: 10.15826/chimtech.2025.12.2.07

CIE coordinate values differ little from the ideal red light (0.66, 0.33).

According to [77], Mn^{2+} ions with a coordination number CN = 4 have close values of radii r = 0.66 Å with Zn^{2+} (r = 0.60 Å), Mg^{2+} (r = 0.56 Å) with the same environment and ion charge. A series of red phosphors was obtained by doping $KMgBO_3$ with Mn^{2+} ions [28]. The structure was solved by the Rietveld method, which showed that the activator ions replace the Mg^{2+} positions. The strong absorption in $KMgBO_3$:Mn^{2+} is explained by the relaxation of the spin- and parity-forbidden d–d transitions of Mn^{2+}. The observed red emission line of Mn^{2+} centered at 636 nm is due to the $^4T_1(^4G) \rightarrow {}^6A_1(^6S)$ transition. The shift of Mn^{2+} emission to the red region of the spectrum is explained by the strong crystal field created by the matrix (Figure 5). The inset shows a photograph of a sample that is excited at 351 nm and emits a bright red color in the dark. The optimal Mn^{2+} content is a concentration of 9 mol.%, and the critical distance is 11.95 Å [28].

Anomal red emission was detected for tetrahedrally coordinated Mn^{2+} in α–$LiZnBO_3$ [51]. The emission spectra of all samples with different activator concentrations contained a road red emission band with a maximum at 647 nm regardless of the excitation wavelength. The authors attribute the red emission with further splitting of the d-level of Mn^{2+} during the transition from the excited electronic state to the ground state $^4T_1$ (^4G) → $^6A_1$ (^6S). Luminescence quenching in the samples was observed at the Mn^{2+} content x = 7 mol %. That is, in α-$LiZnBO_3$:Mn^{2+} there is a weakening of the selection rules for the spin and parity of the *d–d* transitions of the divalent manganese ions. The Zn^{2+} ions are coordinated by O^{2-}, forming a distorted tetrahedron. Substitution of Mn^{2+} ions for the positions of Zn^{2+} ions leads to further distortion of the tetrahedra, creating a strong crystal field, as in the case of CaZnOS.

The absence of dependence of peak positions and the shape of emission spectra on the excitation wavelength indicates the presence of only one luminescence center in the material. This confirms that the activator ions (Mn^{2+}) fill only one position in the lattice of double lithium zinc borate. The observed emission band is explained by the $^4T_1$ (^4G) → $^6A_1$ (^6S) transition of Mn^{2+} ions.

6.4. Tunable luminescence

Along with thermal stability, the most important technological parameter of a phosphor is quantum efficiency (QE), which determines its suitability for use in LEDs. Their use in backlit displays is limited by low quantum efficiency (QE) [4, 5]. Inorganic phosphors with color tuning and excited in the near ultraviolet are required for display backlighting.

The quantum efficiency of luminescence is reduced by nonradiative channels, which can be minimized by using low-phonon host lattices. The internal quantum efficiency has a direct effect on the absorption capacity of the material and the intensity of the radiation. In a luminescent material, the larger the particles, the higher the scattering of the converted light. Accordingly, the higher the absorption losses, which reduce the total number of photons extracted from the luminophore surface. That is, the scattering losses are determined by the size of the phosphor particles and their distribution [4].

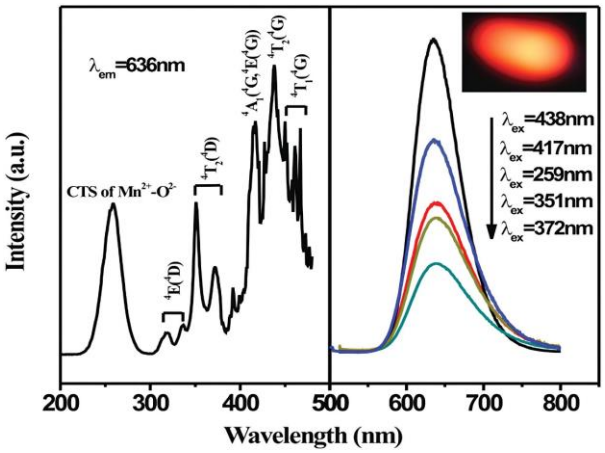

Figure 5 Excitation spectrum at 636 nm and emission spectra excited by different wavelengths of phosphorus $KMgBO_3$:0.09Mn^{2+}, according to [28].

Table 5 Characteristics of emission bands in some red phosphors.

Material	Sr. gr.	λ_{exc}, (nm)	Peak center, (nm)	FWHM (nm)	CIE (x, y)	Ref.
$LiMgBO_3$:0.04Mn^{2+}	C2/c	427	705	–	(0.715, 0.285)	37
α-$LiZnBO_3$:Mn^{2+}	C2/c	431	647	80	(0.66, 0.34)	38
$NaCaBO_3$:Mn^{2+}	Pmmn	347			(0.605, 0.395)	64
$KMgBO_3$:Mn^{2+}	$P2_13$	438	636	70	(0.66, 0.33)	28
β- $Zn_3B_2O_6$:Mn^{2+}	C2/c	587	595	94	(0.559, 0.0439)	32
CaZnOS:Mn^{2+}	$P6_3cm$	300	614	50		76
BaZnOS:Mn^{2+}	CmCm	315	634	60		76
$ZnGeN_2$:Mn^{2+}	$Pna2_1$	343	605	143	(0.6259,0.3662)	78
$Ca_3MgP_4O_{16}$:Mn^{2+}	C12/c1	410	625	120	(0.5964, 0.401)	79
$Ca_8ZnLu(PO_4)_7$:Mn^{2+}	R3c	369	650	–	(0.677, 0.323)	80
$SrZn_2S_2O$:Mn^{2+}	$Pmn2_1$	310	590		(0.559, 0.437)	81

 DOI: 10.15826/chimtech.2025.12.2.07

In a number of single-phase phosphors, it is possible to successfully achieve emission color regulation by co-doping with Ce^{3+}-Tb^{3+}-Mn^{2+} [84,85,90–93] or Ce^{3+}-Eu^{2+}-Mn^{2+} [94], etc. Usually, Ce^{3+}-Tb^{3+} and Ce^{3+}-Mn^{2+} pairs combine well in the energy transfer process due to their matched energy levels [95]. In addition, Eu^{2+} and Ce^{3+} ions are commonly used as sensitizers because their emission bands are so broad that they easily overlap with the excitation band of other activators, such as Mn^{2+} [94].

Tunable luminescence was studied for a number of borates , such as $LiCaBO_3$ [40], $LiBaBO_3$ [41, 42], $NaMgBO_3$ [43], $NaCaBO_3$ [44, 46, 64], and $NaSrBO_3$:Ce^{3+}/Mn^{2+} [45, 65]. Upon excitation with near-UV light, all the studied co-doped samples exhibited double emission of blue and orange (red), which are the result of the 5d–4f transitions in Ce^{3+} ions and the forbidden transition in Mn^{2+} ions. Guo et al. [40] reported that the energy transfer from Ce^{3+} → Mn^{2+} is related to the resonance type and has a dipole–dipole (*d*–*d*) mechanism with a critical distance of about 4.1 Å. It is believed that by regulating the concentration of Ce^{3+} and Mn^{2+} ions, the emission color can be adjusted from blue to orange. Thus, the glow color of $LiBaBO_3$ phosphors: 5 mol.% Ce^{3+}/*y* mol.% Mn^{2+} (*y* = 0, 1, 2, 3, 4, and 5) changed from blue to orange with an increase in the content of manganese ions (see Figure 6). The nonradiative energy transfer process Ce^{3+}→ Ce^{3+} is described by exchange interaction, radiation reabsorption and multipolar interaction [41]. The energy transfer efficiency of Ce^{3+} → Mn^{2+} in the $LiBaBO_3$ lattice contributes to a gradual decrease in the luminescence intensity of the materials with increasing manganese ion content. It is noted that the material of the composition $LiBaBO_3$:5 mol.% Ce^{3+}/2 mol.% Mn^{2+} has a glow close to white light with CIE (0.358, 0.251).

In the sample $NaSrBO_3$:Ce^{3+},Mn^{2+}, the energy transfer efficiency of Ce^{3+} →Mn^{2+} was almost 50%, and the critical distance calculated from spectral data and from the results of crystal structure determination is ~13 Å [45]. In $NaCaBO_3$ phosphors obtained by different methods [44], the color was tuned from blue to red by changing the Ce^{3+}/Mn^{2+} ratio. The samples synthesized by sol-gel technology with grain sizes ~ 5 μm showed the highest energy transfer efficiency (90%) and higher quantum efficiency (80%) than those obtained by solid-phase method. The authors attribute this to the smooth surface, size, and homogeneity of the sensitizer/activator ions. It was observed that nanosize and homogeneous shape of crystals contributes to an increase in their density [74, 98], an increase in the efficiency of the emitted light and the intensity of luminescence [74, 96–99].

The photoluminescent properties of $NaCaBO_3$:Ce^{3+},Mn^{2+} were investigated in detail in [44]. In the emission spectrum of the $NaCa_{0.89}BO_3$:0.01Ce^{3+},0.10Mn^{2+} sample, two bands with maxima at 400 and 600 nm were observed, due to energy transfer from Ce^{3+} to Mn^{2+} with an efficiency of > 83%. The resonance nature of energy transfer by the dipole-dipole mechanism wasestablished. The critical energy transfer distance found by the spectral overlap method is R_C = 19.41 Å, and the one calculated by the concentration quenching method is 22.85 Å.

Varying the concentration of Mn^{2+} in $NaCa_{0.992y}BO_3$:0.01Ce^{3+},*y*Mn^{2+} changed the emission colors from blue CIE (0.162, 0.031) to white light (0.335, 0.259) and orange light (0.489, 0.246).

The structure, morphology, energy transfer mechanism, photoluminescent and temperature-dependent properties of a new series of dual-emitting borates $NaMgBO_3$:Ce^{3+},Mn^{2+} for use in temperature measurement devices were studied [43]. Intense dual broadband emission with two peaks located at 475 and 710 nm was recorded. The first maximum is attributed to the d–f transition of Ce^{3+}, and the second to the $^4T_1$ g(G) → ^{6} A_1g(S) transition of Mn^{2+}.

Temperature-dependent emission of the phosphorus $NaMgBO_3$:Ce^{3+},Mn^{2+} showed thermally stable luminescence of Ce^{3+} and nearly linear thermal quenching curve of Mn^{2+}.

Tunable luminescence was obtained for $NaCaBO_3$:Eu^{2+},Mn^{2+} phosphors by regulating the concentration of Eu^{2+} and Mn^{2+} ions [46]. When excited at 330 nm, two bands at wavelengths of 477 and 602 nm are present in the emission spectrum due to the energy transfer of Eu^{2+} → Mn^{2+}.

The energy transfer is confirmed by the spectral overlap of the $NaCaBO_3$:Eu^{2+} emission band with the $NaCaBO_3$:Mn^{2+} excitation band. It is accompanied by a decrease in the Eu^{2+} emission lifetime with increasing Mn^{2+} concentration. Figure 7 shows the energy transfer model between Ce^{3+}→ Tb^{3+} and Ce^{3+}→ Mn^{2+} in the $NaCaBO_3$ matrix [64].

Ce^{3+} ions absorb ultraviolet light, transitioning from the ground state ($^2F_{5/2}$) to excited states. Then the energy is transferred to the $^5D_3$ level of Tb^{3+} ions, which gives its characteristic transitions and transfers energy to the $^5D_4$ level by cross-relaxation. This is followed by a set of characteristic optical transitions $^5D_4$→^7F_J followed by a radiative transition from the excited state $^4T_1$ (^4G) to the ground state $^6A_1$ (^6S), which leads to the typical Mn^{2+} emission at wavelengths 488, 545, 586 and 623 nm (*J* = 6, 5, 4 and 3) in the matrix lattice.

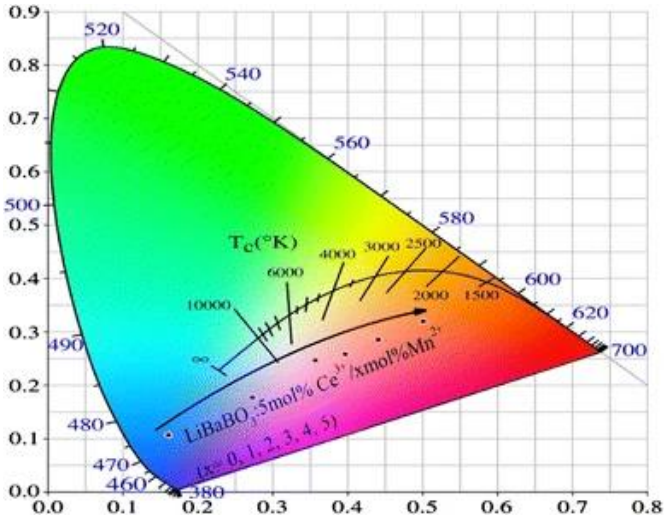

Figure 6 CIE chromaticity diagram of $LiBaBO_3$:5 mol. % Ce^{3+}/*y* mol.% Mn^{2+} (*y* = 0, 1, 2, 3, 4, and 5) [41].

 DOI: 10.15826/chimtech.2025.12.2.07

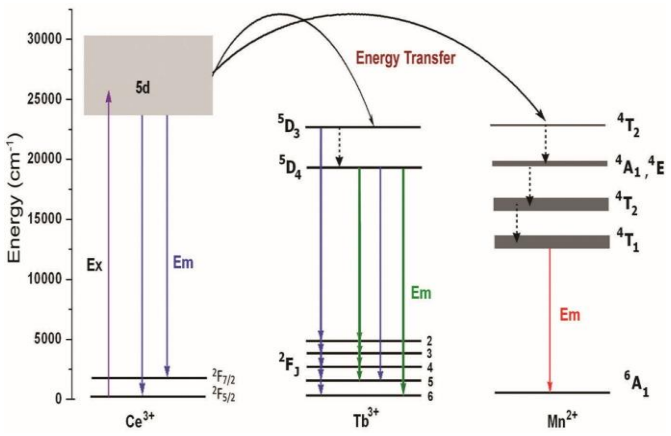

Figure 7 Model of energy transfer between Ce^{3+}→Tb^{3+} and Ce^{3+}→Mn^{2+} in the $NaCaBO_3$ matrix [64].

Variation in the content of co-doped ions showed that with an increase in the concentration of Tb^{3+}, the intensity of Ce^{3+} emission decreases; the intensity of Tb^{3+} emission increases to x = 0.05 and then begins to decrease due to concentration quenching.

The obtained results indicate an efficient energy transfer from Ce^{3+} to Tb^{3+} and the possibility of regulating the intensities of blue Ce^{3+} or green Tb^{3+} emission by appropriately adjusting the concentration of Ce^{3+} (sensitizer) and Tb^{3+} (activator). A similar situation is observed with the energy transfer of Ce^{3+}→ Mn^{2+}. According to the emission spectra of $NaCaBO_3$:0.01Ce^{3+},yMn^{2+} (λ_{ex} = 347 nm) with different concentrations of Mn^{2+}, it was found that the PL intensity of the red band of the Mn^{2+} activator radiation increases and reaches a maximum at 5 mol %, and then the effect of concentration quenching is manifested (Figure 8).

The intensity of the blue fluorescence of the Ce^{3+} sensitizer decreased simultaneously with an increase in the Mn^{2+} content as a result of energy transfer from Ce^{3+} to Mn^{2+}. The energy transfer efficiency (nT) of the sensitizer → activator gradually increases with increasing activator content.

The effects of energy transfer from the sensitizer to the activator caused by rare-earth ions were considered for $NaSrBO_3$:RE (RE = Ce^{3+}, Tb^{3+}, Mn^{2+}) in [65]. It was found that Ce^{3+} ion can be used as a sensitizer transferring its energy through resonance to Tb^{3+} or Mn^{2+} activators.

Energy transfer from the sensitizer to the activator promotes emission of adjustable color; white light emission can be obtained by mixing tricolor (RGB) light sources with suitable component ratios.

Figure 9 shows the compositions and CIE chromaticity coordinates calculated from the emission spectra of the studied phosphors. The insets show these devices at a forward bias current of 20 mA. The authors compared the photoluminescence of phosphors $NaSrBO_3$:RE (RE = Ce^{3+}, Tb^{3+}, Mn^{2+}) with the data obtained for $NaCaBO_3$:RE (RE = Ce^{3+}, Tb^{3+}, Mn^{2+}) [64]. It was shown that the maximum PL emission intensity of $NaSrBO_3$:Ce^{3+} phosphorus is slightly higher than 30% of that of $NaCaBO_3$:Ce^{3+} and the true colors of $NaSrBO_3$:Ce^{3+} (blue) and $NaCaBO_3$:Ce^{3+} (indigo). It was found that $NaSrBO_3$: Ce is more suitable for use in a commercial device based on a UV chip, since it has greater thermal stability. The activation energy of $NaSrBO_3$:Ce is (E_a) ~0.35 eV, while that of $NaCaBO_3$:Ce is (E_a) ~0.26 eV.

Defects in the crystal lattice of luminescent materials (surface defects, atomic vacancies, electrical defects) also lead to low values of internal quantum efficiency. Due to the reduction of surface defects, the distance between the luminescent centers and the extinguishing centers will increase, blocking the non-radiative energy transfer channel to the extinguishing centers.

The quantum efficiency significantly depends on the crystallinity of the substance, the size and morphology of the particles. The concentration of surface defects differs significantly for nanoparticles compared to their bulk counterparts. Surface modification is important for nanoparticles because of their extremely large surface area [98]. Thus, approaches that contribute to the enhancement of internal quantum efficiency should be aimed at reducing the formation of such defects. Table 6 presents for comparison the values of internal (IQE), absolute (QE) and external quantum efficiency (EQE) for doped $MMeBO_3$ and previously studied materials excited by near UV light.

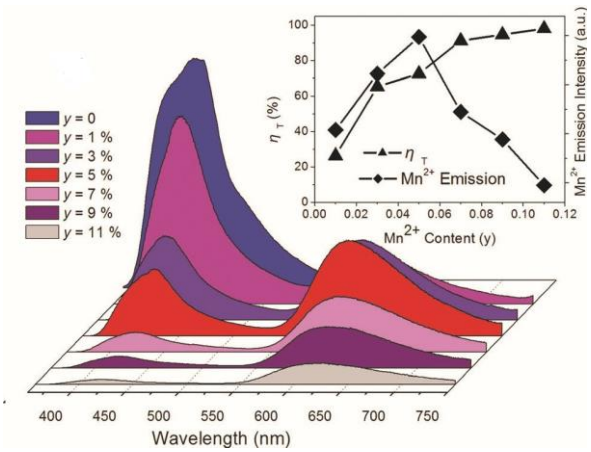

Figure 8 Emission spectra of $NaCaBO_3$:Ce^{3+},yMn^{2+} with different Mn^{2+} content at λ_{ex} = 347 nm [64].

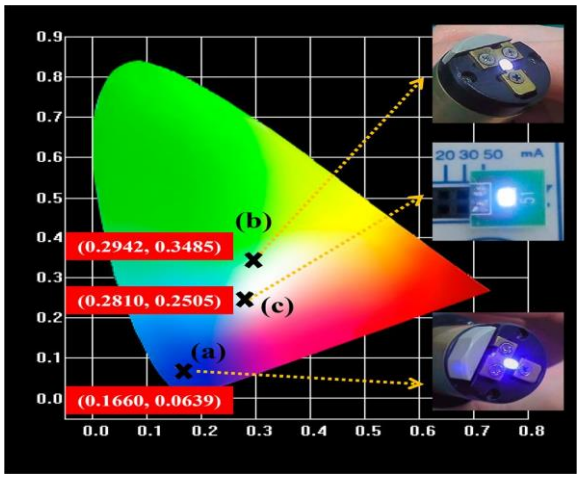

Figure 9 CIE chromaticity coordinates for (a) $NaSr_{0.99}BO_3$:0.01Ce^{3+}; (b) $NaSr_{0.92}BO_3$:0.01Ce^{3+}, 0.07Tb^{3+}; (c) $NaSr_{0.89}BO_3$:0.01Ce^{3+}, 0.07Tb^{3+}, 0.03Mn^{2+} phosphors [65].

 DOI: 10.15826/chimtech.2025.12.2.07

The comparison showed that the values of this parameter for the described borates are not the lowest and can be improved under certain conditions. According to [83], the quantum yield can be improved by optimizing the processing conditions and phosphorus composition by controlling particle sizes, size distribution, morphology, and crystal defects.

Control over particle size and morphology, their regulation by optimization of synthesis methods to change quantum efficiency is reported in [83, 90, 92]. QE can be further increased by soft chemistry methods such as co-precipitation, sol-gel, and hydrothermal [62].

Table 6 Comparison of quantum efficiencies of doped $MMeBO_3$ borates with quantum efficiencies of other typical phosphors.

Material	$\lambda_{exc.}$ (nm)	IQE (%)	QE (%)	EQE (%)	Ref.
$LiMgBO_3$:0.04Mn^{2+}	427	34	–	–	37
α-$LiZnBO_3$:0.07Mn^{2+}	431	44	–	32	38
$KMgBO_3$:0.09 Mn^{2+}	438	–	52	–	28
$LiGd_9(SiO_4)_6O_2$:Mn^{2+}	312	71	–	–	82
$ZnGeN_2$:Mn^{2+}	343	–	23	–	78
$NaCaBO_3$:0.01Ce^{3+}, 0.03Mn^{2+}	360	–	33	–	44
$Mg_2Y_2Al_2Si_2O_{12}$:0.07Ce^{3+} 0.03Mn^{2+}	470	83	-	–	83
$Ca_{11}(SiO_4)_4(BO_3)_2$:0.01Ce^3, 0.03Mn^{2+}	338	-	10	–	84
$Li_2Ca_4Si_4O_{13}$:0.04Ce^{3+}, 0.04Mn^{2+}	365	49	–		85
$Li_2Ca_4Si_4O_{13}$:0.04Ce^{3+}, 0.24Mn^{2+}	365	13	–		85
$CaTiSiO_5$:0.06Ce^{3+}, 0.08Mn^{2+}	320	–	52	–	86
$BaMgSi_4O_{10}$:0.04Eu^{2+}, 0.04Mn^{2+}	310	69	–	48	87
$Ba_3Y(BO_3)_3$:0.20 Eu^{3+}, 0.01Bi^{3+}	393	–	35	–	88
$Ba_9YSi_6O_{24}$:0.02Eu^{3+}, 0.024Bi^{3+}	337	58	–		89
$NaSrBO_3$:0.01Ce^{3+}, 0.07Tb^{3+}	365	71	77	55	65
$NaSrBO_3$:0.01Ce^{3+}, 0.03Mn^2	365	50	69	34	65
$NaSrBO_3$:0.01Ce^{3+}, 0.07Tb^{3+}, 0.03Mn^{2+}	365	63	73	46	65
$NaCaBO_3$:0.01Ce^{3+}	347	–	75	–	64
$NaCaBO_3$:0.01Ce^{3+}, 0.05 Tb^{3+}, 0.03Mn^{2+}	347	–	36	–	64
$Ca_3Al_2O_6$:Ce^{3+}, Tb^{3+}, Mn^{2+}	305		14		90
$Ca_9La(PO_4)_7$:0.15Ce^{3+}, 0.10Tb^{3+}, 0.04Mn^{2+}	290	85	–	69	92
$Ca_3Y(AlO)_3(BO_3)_4$:0.05Ce^{3+}, 0.20Tb^{3+}, 0.02Mn^{2+}	350	54	–	–	93
$Ca_3Gd(AlO)_3(BO_3)_4$:0.05 Ce^{3+}, 0.20Tb^{3+}, 0.02Mn^{2+}	350	43	–		93
$Ca_{11}(SiO_4)_4(BO_3)_2$:0.01Ce^{3+}, 0.03Tb^{3+}, 0.05Mn^{2+}	338	–	13	–	84

7. White LEDs based on $MMeBO_3$ borates

To assess the potential application of the synthesized borates, the authors of a number of studies fabricated devices close to white LEDs by combining the required phosphorus and a chip with a near-UV wavelength (λ = 365–370 nm).

The data from some devices showing color rendering indices (Ra), correlated temperature (CCT), chromaticity coordinates (CIE), and maximum luminance (LE) are shown in Table 7.

According to Zhang et al. [64], the CIE chromaticity coordinates of $NaCaBO_3$:Ce^{3+},Tb^{3+},Mn^{2+} phosphors can be tuned from blue (0.161, 0.107) to red (0.605, 0.395) by controlling the Mn^{2+} content. The color of the same phosphors can be changed from violet to white and then yellow in the visible region of the spectrum by changing the concentration of Tb^{3+}.

Table 7 shows the optimal phosphor composition ($NaCaBO_3$:Ce^{3+}, Tb^{3+}, Mn^{2+}– NCB:0.01Ce^{3+}, 0.05Tb^{3+}, 0.03Mn^{2+}) giving white light with CIE (0.344, 0.313) and its corresponding correlated color temperature.

The white emission of the sample of the specified composition has a lower color temperature and is closer to the ideal white light (0.333, 0.333) compared to the phosphors listed there: CYGB: 0.01Ce^{3+}, 0.07Tb^{3+}, 0.03Mn^{2+}, CSB:0.01Ce^{3+}, 0.03Tb^{3+}, 0.05Mn^{2+}, BMP:0.03Ce^{3+}, 0.03Tb^{3+}, 0.05Mn^{2+}, SYPSO:0.05Ce^{3+}, 0.25Tb^{3+}, 0.25Mn^{2+}.

Figure 10 shows the electroluminescence spectrum of another device made on the basis of $NaCa_{0.96}BO_3$:Ce^{3+},Mn^{2+} [44]. The spectrum clearly shows a blue emission band centered at 400 nm, belonging to the $5d^1$ –$4f^1$- transition of Ce^{3+} ions and an orange band centered at about 600 nm, which corresponds to the $^4T_1(^4G)$ – $^6A_1(^6S)$ transition of Mn^{2+} ions.

It can be seen from Table 6 that the WLED device shows lower color temperature and high color rendering index, not inferior to the NCB described above: 0.01Ce^{3+}, 0.05Tb^{3+}, 0.03Mn^{2+}. In addition, the borate $NaCa_{0.96}BO_3$:0.01Ce^{3+}, 0.03Mn^{2+} exhibits a quantum yield of 33% and a luminous efficacy of 6.2 lm/W when excited at 360 nm.

8. Conclusion

Previous lighting technologies have been replaced by a new generation of light sources - white light-emitting diodes (WLEDs). These are reliable in use, environmentally friendly, and stable during long-term use. They are characterized by efficient light output and low energy consumption. Phosphors based on rare earth elements (REE) are currently used in lighting technology.

 DOI: 10.15826/chimtech.2025.12.2.07

Table 7 Photoelectric characteristics of $NaMeBO_3$-doped (Me = Ca, Sr) devices and some typical white -LED devices.

Material	Device	Current (mA)	R_a	CCT (K)	CIE (*x*, *y*)	LE (Im/W)	Ref.
$NaCa_{0.96}BO_3:Ce^{3+}$, Mn^{2+}	LED chip (370 nm), NCB:0.01Ce^{3+}, 0.03Mn^{2+}	60	91	4046	(0.326, 0.274)	6	44
$NaCaBO_3:Ce^{3+}$, Tb^{3+}, Mn^{2+}	LED nU- chip (370 nm), NCB: 0.01Ce^{3+}, 0.05Tb^{3+}, 0.03Mn^{2+}			4898	(0.344, 0.313)		64
$NaSr_{0.89}BO_3:Ce^{3+}$, Tb^{3+}, Mn^{2+}	InGaN (365 nm) *NSB:0.01Ce^{3+}, 0.07Tb^{3+}, 0.03Mn^{2+}	10	76	8814	(0.2895, 0.2942)	70	65
$NaSr_{0.89}BO_3:Ce^{3+}$, Tb^{3+}, Mn^{2+}	InGaN (365 nm) NSB:0.01Ce^{3+}, 0.07Tb^{3+}, 0.03Mn^{2+}	20	76	9072	(0.2867, 0.2944)	70	65
$NaSr_{0.89}BO_3:Ce^{3+}$, Tb^{3+}, Mn^{2+}	InGaN (365 nm) NSB:0.013Ce^{3+}, 0.073Tb^{3+}, 0.032Mn^{2+}	20			(0.2810, 0.2505)	70	65
$NaSr_{0.89}BO_3:Ce^{3+}$, Tb^{3+}, Mn^{2+}	InGaN (365 nm) NSB:0.01Ce^{3+}, 0.07Tb^{3+}, 0.03Mn^{2+}	30	75			70	65
$NaSr_{0.89}BO_3:Ce^{3+}$, Tb^{3+}, Mn^{2+}	InGaN (365 nm) NSB:0.01Ce^{3+}, 0.07Tb^{3+}, 0.03Mn^{2+}	60	73			70	65
$BaMg_2(PO_4)_2:Ce^{3+}$, Tb^{3+}, Mn^{2+}	LED chip (365 nm), BMP:0.03Ce^{3+}, 0.03Tb^{3+},0.05 Mn^{2+}	–	77	6217	(0.312, 0.313)	–	94
$Ca_3Y(GaO)_3(BO_3)_4$: Ce^{3+}, Tb^{3+}, Mn^{2+}	LED chip (365 nm), CYGB:0.01Ce^{3+},0.07Tb^{3+}, 0.03Mn^{2+}	350	–	6524	(0.31, 0.33)	–	95
$Ca_{11}(SiO_4)(BO_3)_2$: Ce^{3+},Tb^{3+},Mn^{2+}	LED chip (365 nm), CSB:0.01Ce^{3+}, 0.03Tb^{3+}, 0.05Mn^{2+}	–	92	–	(0.303, 0.309)	–	84
$Sr_{3.5}Y_{6.5}O_2(PO_4)_{1.5}(SiO_4)_{4.5}$:$Ce^{3+}$,$Tb^{3+}$, Mn^{2+}	LED nU-chip (370 nm), SYPSO:0.05Ce^{3+},0.25Tb^{3+}, 0.25Mn^{2+}	25	90	6189	(0.320, 0.318)	8	96

*NSB:0.01Ce^{3+},0.07Tb^{3+},0.03Mn^{2+} (*NSB – Material $NaSr_{0.89}BO_3:Ce^{3+}$,Tb^{3+},Mn^{2+}).

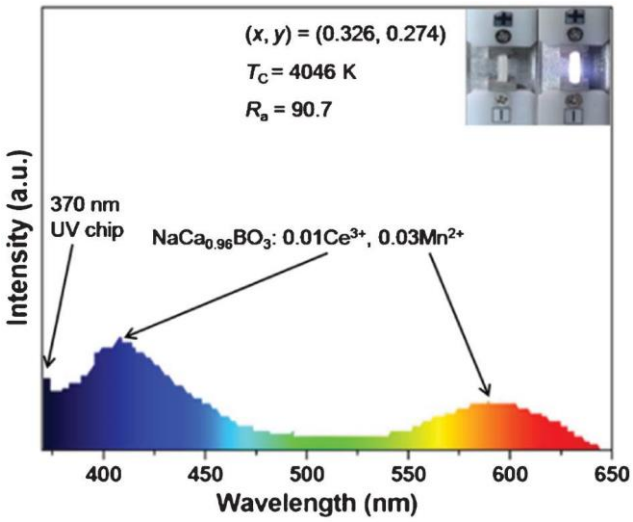

Figure 10 Electroluminescence spectrum of a device based on $NaCa_{0.96}BO_3$:0.01Ce^{3+},0.03Mn^{2+}, controlled by a current of 60 mA [44].

Despite the high characteristics of these phosphors, there is a constant search for new materials due to difficulties in isolating and processing rare earths, as well as their high cost. An alternative to replacing them as activators is transition metals, in particular Mn^{2+} ions and heavy metals such as Bi^{3+}, Pb^{2+}. Co-doping these ions with rare earth elements (REEs) such as Ce^{3+}, Eu^{3+} and Eu^{2+} is also possible. These coactivators have a higher absorption coefficient for 4*f*-to-4*f* transitions than other lanthanides. The excited states of Mn^{2+}, which coincide with the energies of Eu^{2+} and Ce^{3+}, facilitate efficient energy transfer from the co-doped REEs (sensitizers) to the Mn^{2+}(activators). Their co-doping with Mn^{2+} and Bi^{3+} ions enhances the emission intensity and allows rich color tuning. When the inorganic matrix $MMeBO_3$ is co-doped with Ce^{3+} and Mn^{2+} ions, white light can be obtained due to efficient resonance-type energy transfer. Matrices of borate luminophores $MMeBO_3$, containing alkali and alkaline earth metals, as well as zinc, are prepared by a traditional solid-phase method. Oxides, carbonates of the corresponding metals and boric acid are used as initial components. Annealing is carried out in a reducing atmosphere to avoid possible oxidation of ions with variable valence at elevated temperatures. The crystal structures of doped borates are frameworks formed by polyhedra of large metals bonded together by common edges and vertices. Boron-oxygen triangles isolated from each other occupy the voids of this framework.

Alloying additives introduced into the crystal structure lead to its distortion. However, deformations of structures do not lead to its radical restructuring.

Temperature-dependent emission of phosphors $Li_{0.94}M_{0.06}MgBO_3$:0.04Mn^{2+}, M = Li, Na, K; $NaCa_{0.96}BO_3$:0.01Ce^{3+}, 0.03Mn^{2+} excited by UV indicates excellent thermal stability of the materials. Due to the $NaMgBO_3$:0.01Ce^{3+}, 0.06Mn^{2+} relatively high temperature resolution of 0.01 K, the phosphor can find application in optical thermometry.

Doped with Mn^{2+} ions, the phosphors $LiMgBO_3$, α-$LiZnBO_3$, $NaCaBO_3$ and $KMgBO_3$, revealed the presence of emission bands in the red region of the spectrum. The values of CIE chromaticity coordinates of α-$LiZnBO_3$ and $KMgBO_3$ almost coincide with the CIE values of ideal red light (0.66, 0.33). Near-UV excited phosphors with color tuning and high quantum efficiency values are in demand for use in full-color displays. The borate materials under

 DOI: 10.15826/chimtech.2025.12.2.07

consideration meet these requirements since they show not the lowest quantum efficiency values compared to other inorganic materials. In some cases, for example, for $NaSrBO_3$:0.01 Ce^{3+},0.07Tb^{3+} and $KMgBO_3$:0.09Mn^{2+} these parameters are even higher than the average values (see Table 6)

Considering the dependence of quantum efficiency on the degree of crystallinity, morphology and particle size, it is possible to correct this parameter by selecting and optimizing the required method of synthesizing phosphors. Prefabrication of devices based on activated borates $NaCa_{0.96}BO_3$:Ce^{3+}, Mn^{2+} [44], NCB:0.01Ce^{3+}, 0.05Tb^{3+},0.03Mn^{2+} [64], $NaSr_{0.89}BO_3$:Ce^{3+}, Tb^{3+}, Mn^{2+} [65] can give light close to white. The best value of CIE color coordinates (0.344, 0.313) and its corresponding correlated color temperature of 4898 K was demonstrated by the sample LED nU- chip (370 nm), NCB:0.01Ce^{3+}, 0.05Tb^{3+}, 0.03Mn^{2+} [64].

Co-doping with rare-earth metal ions as sensitizers, using pairs of activators Ce^{3+}/Mn^{2+}, Eu^{2+}, Mn^{2+}, Eu^{3+}/Bi^{3+}, Ce^{3+}- Tb^{3+}- Mn^{2+} allows to significantly increase the luminescence efficiency, as well as to tune the emission color in a wide range from blue to orange due to the energy transfer from the sensitizer to the activator by changing their concentration.

Thus, the analysis of the literature showed that borates of the general composition $MMeBO_3$ (M = Li, Na, K; Me = Mg, Ca, Sr, Ba, Zn), doped with Mn^{2+}, Bi^{3+} and co-doped with Ce^{3+}, Eu^{2+}, Eu^{3+} can be considered as very promising luminescent materials. They can find application as phosphors for near-UV and UV light-emitting diodes and field-emission displays.

At the same time, despite numerous studies and promising applications of the studied phosphors, many questions remain unresolvedж in particular, it can be noted that the quantum efficiency is not sufficiently high and the correlated temperatures of some materials are relatively high. Therefore, further systematic research and development is required in this area.

Supplementary materials

No supplementary materials are available.

Acknowledgments

None.

Author contributions

Conceptualization and methodology: T.N.
Data curation and Formal Analysis: A.V.
Writing—original draft: A.V, T.N.
Writing–review & editing: T.N.

Conflict of interest

The authors declare no conflict of interest.

Additional information

Author IDs:
Tatyana Khamaganova, Scopus ID 6602131345;
Alexandra Logvinova, Scopus ID 57197825558.

Website:
Baikal Institute of Nature Management Siberian branch of the Russian Academy of sciences, https://www.binm.ru/.

A list of 10 most significant cited papers

1. Chen L, Chu C-I, Liu R-S. Improvement of emission efficiency and color rendering of high-power LED by controlling size of phosphor particles and utilization of different phosphors. Microelectron Reliab. 2012;52:900–904. doi:10.1016/j.microrel.2011.07.058
2. Wu L, Bai Y, Wu L, Yi H, Zhang X, Zhang L, Kong Y, Zhang Y, Xu J. Analysis of the structure and abnormal photoluminescence of a red-emitting $LiMgBO_3$:Mn^{2+} phosphor. Dalton Trans. 2018;47:13094–13105. doi:10.1039/C8DT02450
3. Tian J, Xie J, Zhuang W. Recent Advances in Multi-Site Luminescent Materials: Design, Identification and Regulation. Mater. 2023;16:2179. doi:10.3390/ma16062179
4. Lin CC, Liu Y-P, Xiao ZR, Wang Y-K, Cheng B-M, Liu R-S. All-In-One Light-Tunable Borated phosphors with Chemical and Luminescence Dynamical Control Resolution. ACS Appl Mater Interfaces. 2014;6:9160–9172. doi:10.1021/am501232y
5. Zhang X, Gong M. Single-phased white-light-emitting $NaCaBO_3$:Ce^{3+},Tb^{3+}, Mn^{2+} phosphors for LED applications. Dalton Trans. 2014;43:2465–2472. doi:10.1039/c3dt52328d
6. Wu L, Wang B, Zhang Y, Li L, Wang HR, Yi H, Kong YF, Xu JJ. Structure and photoluminescence properties of a rare-earth free red-emitting Mn^{2+}-activated $KMgBO_3$. Dalton Trans. 2014;43:13845. doi:10.1039/c4dt01524j
7. Wang H, Wu L, Yi H, Wang B, Wu L, Gua Y, Zhang Y. Abnormal luminescent property of Mn^{2+} in α-$LiZnBO_3$:Mn^{2+}. Dalton Trans. 2015;44:1427–1434. doi:10.1039/c4dt02626h
8. Liang Z, Mo F, Zhang X, Zhoun L. Luminescence of the $LiMgBO_3$:Eu^{3+},Bi^{3+} phosphor. J Lumin. 2014;151:47–51. doi:10.1016/j.jlumin.2014.02.001
9. Guo C, Yu J, Ding X, Lai M, Ren Z, Bai J. A dual-emission phosphor $LiCaBO_3$:Ce^{3+}, Mn^{2+} with energy transfer for near-UV LEDs. J Electrochem Soc. 2011;158:42–46. doi:10.1149/1.3526319
10. Lephoto MA, Tshabalala KG, Motloung SJ, Shaat SKK, Ntwaeaborwa OM. Tunable emission from $LiBaBO_3$:Eu^{3+}, Bi^{3+} phosphor for solid-state lighting. J Lumin. 2017;32:1084–1091. doi:10.1002/bio.3295

References

1. Blasse G, Grabmaier B.C. A general introduction to luminescent materials, Luminescent Materials. Berlin Heidelberg: Springer-Verlag; 1994. 232 p. doi:10.1007/978-3-642-79017-1_1
2. Nakamura S, Fasol G. The Blue Laser Diode. Berlin: Springer; 1997. 343 p.doi:10.1007/978-3-662-03462-0
3. Ma C, Chen H, Luo M, Duan F, Ding Y, Han Y, Zheng T, Yang Y, Xiao Y. A novel borate phosphor $Lu_5Ba_6B_9O_{27}$:Ce^{3+} codoped with Sr^{2+}/Tb^{3+} for NUV-white light emitting diode application. Dalton Trans. 2024;53:14153–14162. doi:10.1039/D4DT01843
4. Smet PF, Parmentier AB, Poelman D. Selecting conversion phosphors for white light-emitting diodes. J Electrochem Soc. 2011;158:37–54. doi:10.1149/1.3568524
5. Chen L, Chu.C.-I, Liu R-S. Improvement of emission efficiency and color rendering of high-power LED by controlling size of phosphor particles and utilization of different phosphors. Microelectron. Reliab. 2012;52:900–904. doi:10.1016/j.microrel.2011.07.058
6. George N.C, Brgoch J, Pell A.J, Cozzan C, Jaffe A, Dantelle G, Llobet A, Pintacuda G, Seshadri R, Chmelka B.F. Correlating local compositions and structures with the macroscopic opti-

cal properties of Ce^{3+}-doped $CaSc_2O_4$, an efficient green-emitting phosphor. Chem Mater. 2017;29:3538–3546. doi:10.1021/acs.chemmater.6b05394
7. Chen X, Yuan X, Xiao W, Song X. Two new rare-earth oxyborates $Ba_4BiTbO(BO_3)_4$ and $Ba_{1.54}Sr_{2.46}BiTbO(BO_3)_4$ and luminescence properties of the $Ba_4BiTb_{1-x}Eu_xO(BO_3)_4$ phosphors. RSC Adv. 2024;14:6270–6284. doi:10.1039/d3ra08265b
8. Hua H, Feng S, Ouyang Z, Shao H, Qin H, Ding H, Du Q, Zhang Z, Jiang J, Jiang H. YAGG:Ce transparent ceramics with high luminous efficiency for solid-state lighting application. J Adv Ceram. 2019;8:389–398. doi:10.1007/s40145-019-0321-9
9. Li J, Yan J, Wen D, Khan W.U, Shi J, Wu M, Su Q, Tanner P.A. Advanced red phosphors for white light-emitting diodes. J Mater Chem C. 2016;4:8611. doi:10.1039/c6tc02695h
10. Khan S, Parauha Y. P, Halwar D.K, Dhoble S.J. Rare Earth (RE) doped color tunable phosphors for white light emitting diodes. J Phys Conf Ser Int Conf Res Front Sci. 2021;1913:012017. doi:10.1088/1742-6596/1913/1/012017
11. Tian J, Xie J, Zhuang W. Recent Advances in Multi-Site Luminescent Materials: Design, Identification and Regulation. Mater. 2023;16:2179. doi:10.3390/ma16062179
12. Ni J, Zhou ZZ, Xu XK, Liu Q, Shen FR, He LH. Probing into Dopant Concentration Dependent Luminescence Properties of Transition Metal Mn^{2+} Activated Ca- α-SiAlON Orange-Red Phosphors. Mod App Mater Sci. 2020;2:276–284. doi:10.32474/MAMS.2020.02.000146
13. Sharma SK, James J, Gupta SK, Hussain S. UV-A,B,C Emitting Persistent Luminescent Materials. Mater. 2022;16:236. doi:10.3390/ma16010236
14. Götze J. Potential of cathodoluminescence (CL) microscopy and spectroscopy for the analysis of minerals and materials. Anal Bioanal Chem. 2002;374:703–708. doi:10.1007/s00216-002-1461-1
15. Verma S, Verma K, Kumar D, Chaudhary B, Som S, Sharma V, Kumar V, Swart H. C. Recent advances in rare earth doped alkali-alkaline earth borates for state lighting applications. Phys B. 2018;535:106–113. doi:10.1016/j.physb.2017.06.073
16. Cantarano A, Ibanez A, Dantelle G. Garnet-type nanophosphors for white LED lighting. Front Mater. 2020;7:210. doi:10.3389/fmats.2020.00210
17. Ling J, Zhou Y, Xu W, Lin H, Lu S, Wang B, Wang K. Red-emitting YAG:Ce,Mn transparent ceramics for warm WLEDs application. J Adv Ceram. 2020;9:45–54. doi:10.1007/s40145-019-0346-0
18. Zhang JC, Wang XS, Yao X. Enhancement of luminescence and afterglow in $CaTiO_3:Pr^{3+}$ by Zr substitution for Ti. J Alloys Compd. 2010;498:152–156. doi:10.1016/j.jallcom.2010.03.138
19. Shi R, Ning L, Wang Z, Chen J, Sham T.-K, Huang Y, Qi Z, Li C, Q. Tang Q, Liang H. Zero-Thermal Quenching of Mn^{2+} Red Luminescence via Efficient Energy Transfer from Eu^{2+} in $BaMgP_2O_7$. Adv Optical Mater. 2019;1901187. doi:10.1002/adom.201901187
20. Shablinskii AP, Povolotskiy AV, Yuriev AA, Biryukov YP, Bubnova RS, Avdontceva MS, Janson SY, Filatov SK. Novel Red-Emitting $BaBi_2B_4O_{10}:Eu^{3+}$ Phosphors: Synthesis, Crystal Structure and Luminescence. Symmetry. 2023;15:918. doi:10.3390/sym15040918
21. Bedyal A.K, Kumar V, Ntwaeaborwa O.M, Swart H.C. A promising orange-red emitting nanocrystalline $NaCaBO_3$: Sm^{3+} phosphor for solid state lightning. Mater Res Express. 2014;1:015006–015012. doi:10.1088/2053-1591/1/1/015006
22. Shao Q, Ding H, Yao L, Xu J, Liang C, Jiang J. Photoluminescence properties of a $ScBO_3:Cr^{3+}$ phosphor and its applications for broadband nearinfrared LEDs. RSC Adv. 2018;8:12035. doi:10.1039/c8ra01084f
23. Jia Z, Yuan C, Liu Y, Wang X.-J, Sun P, Wang L, Jiang H, Jiang J. Strategies to approach high performance in Cr^{3+}-doped phosphors for high-power NIR-LED light sources. Light Sci Appl. 2020;9:86. doi:10.1038/s41377-020-0326-8
24. Adachi S. Photoluminescence Properties of Cr^{3+}-Activated Oxide Phosphors. ECS J Solid State Sci Technol. 2021;10:026001. doi:10.1149/2162-8777/abdc01
25. Palumbo D.T, Brown J.J. Electronic States of Mn^{2+}-Activated Phosphors. J Electrochem Soc. 1970;117(9):1184–1188. doi:10.1149/1.2407765
26. Li Y, Qi S, Li P, Wang Z. Research progress of Mn doped phosphors. RSC Adv. 2017;7:38318. doi:10.1039/c7ra06026b
27. Jiang X, Pan Y, Huang S, X.i'an C, Wang J, Liu G. Hydrothermal synthesis and photoluminescence properties of red phosphor $BaSiF_6:Mn^{4+}$ for LED applications. J Mater Chem C. 2014;2:2301. doi:10.1039/c3tc31878h
28. Wu L, Wang B, Zhang Y, Li L, Wang H. R, Yi H, Kong YF, Xu JJ. Structure and photoluminescence properties of a rare-earth free red-emitting Mn^{2+}-activated $KMgBO_3$. Dalton Trans. 2014;43:13845. doi:10.1039/c4dt01524j
29. Kim JS, Kim Js, Kim T.W, Kim SM., Park HL. Correlation between the crystalline environment and optical property of Mn^{2+} ions in $ZnGa_2O_4:Mn^{2+}$ phosphor. Appl Phys Lett. 2005;86:91912–91913. doi:10.1063/1.1869550
30. Liu C, Zhu X, Zhou Z. Effects of composition modulation on the Structural and luminescence properties of Mn^{2+} doped $Na_2Mg_{1-x}Ca_xSiO_4$ green-emitting phosphors. Optik. 2019;179:875–882. doi:10.1016/j.ijleo.2018.10.076
31. Shang M, Li G, Yang D, Kang X. $(Zn,Mg)_2GeO_4:Mn^{2+}$ submicrorods as promising green phosphors for field emission displays: hydrothermal synthesis and luminescence properties. Dalton Trans. 2011;40:9379–9387. doi:10.1039/c2dt30670k
32. Shi Y, Wen Y, Que M, Zhu G, Wang Y. Structure, photoluminescent and cathodoluminescent properties of a rare-earth free red emitting β-$Zn_3B_2O_6:Mn^{2+}$ phosphor. Dalton Trans. 2014;43:2418–2423. doi:10.1039/C3DT52405A
33. Dai H, Li S, Li Z, Li J, Xin S, Wang C, Zhu G, Dong B. Novel rare earth free phosphors $CsMg_2P_3O_{10}:Mn^{2+}$ with efficient and ultra-broadband red emission for plant growth LEDs. J Am Ceram Soc. 2022;105(7):4719–4730. doi:10.1111/jace.18386
34. Dai L, Torche A, Strelow C, Kipp T, Vuong TH, Rabeah J, Oldenburg K, Bester G, Mews A, Klinke C, Lesyuk R. Role of magnetic coupling in photoluminescence kinetics of Mn^{2+}-doped ZnS nanoplatelets. ACS Appl Mater Interfaces. 2022;14:18806–18815. doi:10.1021/acsami.1c25191
35. Tretyakov Yu.D, Lepis H. Ximiya i texnologiya tverdofazny`x materialov [Chemistry and technology of solid-phase materials], MGU: Moscow; 1985. 253 p. (In Russ.).
36. Lee S, Choi J.I, Kim YJ, Han JK, Ha J, Novitskaya E, Talbot JB, McKittrick J. Comparison of luminescent properties of $Y_2O_3:Eu^{3+}$ and $LaPO_4:Ce^{3+}$, Tb^{3+} phosphors prepared by various synthetic methods. Mater Charact. 2015;103:162–169. doi:10.1016/j.matchar.2015.03.027
37. Wu L, Bai Y, Wu L, Yi H, Zhang X, Zhang L, Kong Y, Zhang Y, Xu J. Analysis of the structure and abnormal photoluminescence of a red-emitting $LiMgBO_3:Mn^{2+}$ phosphor. Dalton Trans. 2018;47:13094–13105. doi:10.1039/C8DT02450
38. Wang H, Wu L, Yi H, Wang B, Wu L, Gua Y, Zhang Y. Abnormal luminescent property of Mn^{2+} in α-$LiZnBO_3:Mn^{2+}$. Dalton Trans. 2015;44:1427–1434. doi:10.1039/c4dt02626h
39. Liang Z, Mo F, Zhang X, Zhoun L. Luminescence of the $LiMgBO_3:Eu^{3+},Bi^{3+}$ phosphor. J Lumin. 2014;151:47–51. doi:10.1016/j.jlumin.2014.02.001
40. Guo C, Yu J, Ding X, Lai M, Ren Z, Bai J. A dual-emission phosphor $LiCaBO_3:Ce^{3+}$, Mn^{2+} with energy transfer for near-UV LEDs. J Electrochem Soc. 2011;158:42–46. doi:10.1149/1.3526319
41. Li J, Li X, Xing H-W, Zhang Y-Z, Yang A-M, Pan Y-H, Liu W-X. Solid state synthesis of $LiBaBO_3:Ce^{3+}/Mn^{2+}$ Phosphors and tunable luminescence induced by energy transfer from Ce^{3+} to Mn^{2+}. J Mater Sci Mater Electron. 2017;28:4738–4743. doi:10.1007/s10854-016-6117-6
42. Lephoto M.A, Tshabalala K.G, Motloung S. J, Shaat S.K.K. and Ntwaeaborwa O.M. Tunable emission from $LiBaBO_3:Eu^{3+},Bi^{3+}$ phosphor for solid-state lighting. J Lumin. 2017;32:1084–1091. doi:10.1002/bio.3295

 DOI: 10.15826/chimtech.2025.12.2.07

43. Song J, Zhao.W, Zhang H, Hao Y.L, Yang H. H, Zhang H, Zhong J. Energy transfer and ratiometric Temperature sensing based on the dual-emitting $NaMgBO_3:Ce^{3+},Mn^{2+}$ phosphor. J Lumin. 2021;232:117858. doi:10.1016/j.jlumin.2020.117858
44. Sun J, Lian Z, Shen G.and Shen D. Blue–white–orange color-tunable luminescence of Ce^{3+}/Mn^{2+}-codoped $NaCaBO_3$ via energy transfer: potential single-phase white-light-emitting phosphors. RSC Adv. 2013;3:1839. doi:10.1039/c3ra42554a
45. Zhang X.G, Zhou L.Y, Gong M.L. Luminescence properties of dual-emission Ce^{3+},Mn^{2+} doped $NaSrBO_3$ phosphors. ECS J Solid State Sci Technol. 2013;2:83–86. doi:10.1149/2.011305jss
46. Wang Y, Zhang H, Wei Q, Su C, Zhang D. Solid state synthesis, tunable luminescence and thermal stability of $NaCaBO_3:Eu^{2+}/Mn^{2+}$ phosphors. Ceram Int. 2016;42:12422–12426. doi:10.1016/j.ceramint.2016.04.182
47. Khamaganova TN. Preparation, luminescence, and application of $LiMeBO_3$ borates, Me = Mg, Ca, Sr, Ba, Zn, Cd. Condensed Matter Interphases. 2023;25(3):311–332. doi:10.17308/kcmf.2023.25/11256
48. Norrestam R. The crystal structure of monoclinic $LiMgBO_3$. Z Kristallogr. 1989;187:103–110. doi:10.1524/zkri.1989.187.1-2.103
49. Wu L, Chen XL, Li H, He M, Dai L, Li XZ, Xu YP. Structure determination of a new $LiCaBO_3$. J Solid State Chem. 2004;177:1111–1116. doi:0.1016/j.jssc.2003.10.018
50. Cheng W-D, Zhang H, Lin Q-S, Zheng F-K, Chen J-T. Syntheses, Crystal and Electronic Structures, and Linear Optics of $LiMBO_3$ (M = Sr, Ba) Orthoborates. Chem Mater. 2001;13:1841–1847. doi:10.1021/cm000808i
51. Chen X, Yang C, Chang X, Zang H, Xiao W. Synthesis and characterization of two alkali – metal zinc borates, α – $LiZnBO_3$ and $Li_{0,48}Na_{0,52}ZnBO_3$. Solid State Sci. 2009;11:2086–2092. doi:10.1016/j.solidstatesciences.2009.08.024
52. Wu L, Zhang Y, Kong YF, Sun TQ, Xu JJ, Chen XL. Structure Determination of Novel Orthoborate $NaMgBO_3$: A Promising Birefringent Crystal. Inorg Chem. 2007;46:5207–5211. doi:10.1021/ic062429i
53. Wu L, Chen XL, Li XZ, Dai L, Xu YP, Zhao M. Synthesis and ab initio X-ray powder diffraction structure of the new alkali and alkali earth metal borate $NaCa(BO_3)$. Acta Crystallogr C. 2005;61:32–34. doi:10.1107/S010827010401964X
54. Wu L, Chen XL, Zhang Y, Kong YF, Xu JJ, Xu YP. Ab initio structure determination of novel borate $NaSrBO_3$. J Solid State Chem. 2006;179:1219–1224. doi:10.1016/j.jssc.2006.01.003
55. Tu J-M, Keszler DA. $BaNaBO_3$. Acta Crystallogr C. 1995;51:1962–1964. doi:10.1107/S010827019400750X
56. Kononova NG, Kokh AE, Bekker TB, Furmanova NG, Maksimov BA, Molchanov VN, Fedorov PP. Growth and Structure of Barium Sodium Orthoborate $NaBaBO_3$ Crystals. Crystallogr Rep. 2003;48:1044–1046. doi:10.1134/1.1627446
57. Wu L, Sun JC, Zhang Y, Jin SF, Kong YF, Xu JJ. Structure determination and relative properties of novel chiral orthoborate $KMgBO_3$. Inorg Chem. 2010;49:2715–2720. doi:10.1021/ic901963t
58. Reddy AA, Das S, Ahmad S, Babu SS, Ferreira JMF, Prakash GV. Influence of the annealing temperatures on the photoluminescence of $KCaBO_3:Eu^{3+}$ phosphor. RSC Adv. 2012;2:8768–8776. doi:10.1039/C2RA20866K
59. Wang Z, Jing Q, Zhang M, Pan S, Yang Z, Zhang H. $(MMgBO_3)n$ (n = 1, M = Li, Na, K, Rb and n = 4, M = Cs): An investigation on the structure transition and optical properties. Inorg Chem Commun. 2014;49:63–67. doi:10.1016/j.inoche.2014.09.022
60. Pan Z, Chen J, Wu H, Li W. Red emission enhancement in Ce^{3+}/Mn^{2+} co-doping suited garnet host $MgY_2Al_4SiO_{12}$ for tunable warm white LED. Opt Mater. 2017;72:257–264. doi:10.1016/j.optmat.2017.06.012
61. Chen H, Wang Y. Photoluminescence and cathodoluminescence properties of novel rare-earth free narrow-band bright green-emitting $ZnB_2O_4:Mn^{2+}$ phosphor for LEDs and FEDs. Chem Eng J. 2018;361:314–321. doi:10.1016/j.cej.2018.12.039
62. Jiao M, Jia Y, Lü W, Lv W, Zhao Q, Shao B, You H. Single-phase white-emitting $Ca_2SrAl_2O_6:Ce^{3+},Li^+$, Mn^{2+} phosphor with energy transfer for UV-excited WLEDs. Dalton Trans. 2014;43:3202. doi:10.1039/c3dt52832d
63. Wei R, Wang L, Hu F, Lib X, Peng X, Shi Y, Guo H, Qiu J. Tunable emission and energy transfer in single-phased $Ba_9Lu_2Si_6O_{24}:Bi^{3+},Eu^{3+}$ for UV W-LEDs. J Lumin. 2018;197:291–296. doi:10.1016/j.jlumin.2018.01.033
64. Zhang X, Gong M. Single-phased white-light-emitting $NaCaBO_3:Ce^{3+},Tb^{3+}$, Mn^{2+} phosphors for LED applications. Dalton Trans. 2014;43:2465–2472. doi:10.1039/c3dt52328d
65. Lin CC, Liu Y-P, Xiao ZR, Wang Y-K, Cheng B-M, Liu R-S. All-In-One Light-Tunable Borated phosphors with Chemical and Luminescence Dynamical Control Resolution. ACS Appl Mater Interfaces. 2014;6:9160–9172. doi:10.1021/am501232y
66. Dexter DL. A Theory of Sensitized Luminescence in Solids. J Chem Phys. 1953;21:836–850. 10.1063/1.1699044
67. Ding J, Wu Q. Recent advances in Bi^{3+}-activated narrow-band emitting phosphors for backlight display applications. Dalton Trans. 2024;3:15403–15411. 10.1039/D4DT01818D
68. Wu S, Xiong P, Liu X, Fu Y, Liu Q, Chao Y, Dong Q, Li Y, Chen W, Chen Y, Ma Z, Peng M. $Sr_3Y(BO_3)_3:Bi^{3+}$ phosphor with excellent thermal stability and color tunability for near-ultraviolet white-light LEDs. Mater Chem C. 2021;9:3672–3681. doi:10.1039/dotc05960a
69. Sun R, Zhao J, Lu J, Su S, Liu R, Lei Z, Hu C, Teng B, Li J, Sun S, Zhong D. Synthesis and characterizations of a color tunable single-phased warm white phosphor $Sr_3Lu(BO_3)_3:Bi^{3+},Eu^{3+}$. J Lumin. 2023;255:119570. doi:10.1016/j.jlumin.2022.119570
70. Sohn K-S, Cho B, Park HD. Photoluminescence behavior of Ti-doped Zn_2SiO_4 thin film phosphors. J Am Ceram Soc. 1999;82:2779–2784. doi:10.1111/j.1151-2916.1999.tb02155.x
71. Rao RP. Tb^{3+} Activated Green Phosphors for PDP Application. J Electrochem Soc. 2003;150:165–171. doi:10.1149/1.1583718
72. Jung KY, Lee DY, Kang YC, Park SB. Size-Dependent Luminescent Properties of Hollow and Dense $BaMgAl_{10}O_{17}$:Eu Blue Phosphor Particles Prepared by Spray Pyrolysis. Kor J Chem Eng. 2004;21:1072–1080. doi:10.1007/BF02705595
73. Culubrk S, Antic Z, Marinovic-Cincovic M, Ahrenkiel PS, Dramicanin MD. Synthesis and luminescent properties of rare-earth (Sm^{3+} and Eu^{3+}) doped $Gd_2Ti_2O_7$ pyrochlore nanopowders. Opt Mater. 2014;37:598–606. doi:10.1016/j.optmat.2014.08.001
74. Wang W, Widiyastuti W, Ogi T, Lenggoro I, Okuyama K. Correlations between crystallite/particle size and photoluminescence properties of submicrometer phosphors. Chem Mater. 2007;19:1723–1730. doi:10.1021/cm062887p
75. Pekgozl I, Erdogmus E, Cubuk S, Basak AS. Synthesis and photoluminescence of $LiCaBO_3$: M(M:Pb^{2+} and Bi^{3+}) phosphor. J Lumin. 2012;132:1394–1399. doi:10.1016/j.jlumin.2012.01.001
76. Duan CJ, Delsing ACA, Hintzen HT. Photoluminescence Properties of Novel Red-Emitting Mn^{2+}-Activated MZnOS (M = Ca, Ba) Phosphors. Chem Mater. 2009;21:1010–1016. doi:10.1021/cm801990r
77. Shannon RD. Revised effective ionic radii and systematic studies of interatomic distances in halides and chalcogenides. Acta Crystallogr A. 1976;32:751–767. doi:10.1107/S0567739476001551
78. Shang M, Wang J, Fan J, Lian H, Zhang Y, Lin J. $ZnGeN_2$ and $ZnGeN_2:Mn^{2+}$ phosphors: hydrothermal-ammonolysis synthesis, structure and luminescence properties. J Mater Chem C. 2015;3:9306. doi:10.1039/c5tc01864a
79. Cao R, Shi Z, Quan G, Hu Z, Zheng G, Chen T, Guo S, Ao H. Rare-earth free broadband $Ca_3Mg_3P_4O_{16}:Mn^{2+}$ red phosphor: Synthesis and luminescence properties. J Lumin. 2018;194:542–546. doi:10.1016/j.jlumin.2017.10.079
80. Yan J, Zhang Z, Wen D, Zhou J, Xu Y, Li J, Ma C.-G, Shi J, Wu M. Crystal structure and photoluminescence tuning of novel

single-phase $Ca_8ZnLu(PO_4)_7:Eu^{2+},Mn^{2+}$ phosphors for near-UV converted white light-emitting diodes. J Mater Chem C. 2019;7:8374–8382. doi:10.1039/c9tc02494h
81. Ma R, Mao S, Wang C, Shao Y, Wang Z, Wang Y, Qu S, Peng D. Luminescence in Manganese (II)-Doped $SrZn_2S_2O$ Crystals From Multiple Energy Conversion. Front Chem. 2020;8:752. doi:10.3389/fchem.2020.00752
82. Zhang Y, Mei L, Liu H, Chang J-C, Liu W-R, Huang Z. Thermal-stable and high-efficient orange-red emitting orthosilicate phosphors $LiGd_9(SiO_4)_6O_2:Mn^{2+}$ for n-UV-pumped w-LEDs. Mater Chem Phys. 2019;228:215–220. doi:10.1016/j.matchemphys.2019.02.079
83. Wang Z, Wang Z, Li Y, Liu J, Bao Q, Meng X, Qiu K, Yang Z, Wang D, Li P. A novel red-emitting phosphor $Mg_2Y_2Al_2Si_2O_{12}:Ce^{3+}/Mn^{2+}$ for blue chip-based white LEDs. RSC Adv. 2021;11:2706–2717. doi:10.1039/d0ra09289d
84. Hou J, Liu J, Zou J, Zhao G, Liu Y, Feng X.-F, Fang Y. High color rendering white light emission from single-phased $Ca_{11}(SiO_4)_4(BO_3)_2:Ce^{3+}$, Tb^{3+}, Mn^{2+} phosphor for UV-based light emitting diodes. J Mater Sci Mater Electron. 2018;29:18807–18814. doi:10.1007/s10854-018-0006-0
85. Kang X, S. Lu S, Wang H, Ling D, Lü W. Tricolor- and White Light–Emitting $Ce^{3+}/Tb^{3+}/Mn^{2+}$-Coactivated $Li_2Ca_4Si_4O_{13}$ Phosphor via Energy Transfer. ACS Omega. 2018;3:16714–16720. doi:10.1021/acsomega.8b01952
86. Cao R, Lao Y, Wang X, Ouyang X, Chen T, Wan H, Fan TS, Xie S. Tunable Emission Properties of $CaTiSiO_5:Ce^{3+}$, Mn^{2+} Phosphor via Efficient Energy Transfer. J Electron Mater. 2020;49:3869–3876. doi:10.1007/s11664-020-08100-2
87. Zhong J, Zhuo Y, Hariyani S, Zhao W, Zhuang W, Brgoch J. Thermally Robust and Color-Tunable Blue-Green-Emitting $BaMgSi_4O_{10}:Eu^{2+},Mn^{2+}$ Phosphor for Warm-White LEDs. Inorg Chem. 2020;59:13427–13434. doi:10.1021/acs.inorgchem.0c01803
88. Li Q, Chen C, Shen B, Yu B, Zhang Y. Enhanced red emission and high thermal stability from Bi^{3+}/Eu^{3+} co-doped $Ba_3Y(BO_3)_3$ phosphors for WLEDs application. J Lumin. 2021;237: 118196. doi:10.1016/j.jlumin.2021.118196
89. Guo H, Zheng Z, Teng L, We Ri, Hu F. Tunable white-light emission and energy transfer in single-phase Bi^{3+},Eu^{3+} co-doped $Ba_9Y_2Si_6O_{24}$ phosphors for UV w-LEDs. J Lumin. 2019;213:494–503. doi:10.1016/j.jlumin.2019.05.057
90. Zhang J, He Y, Qiu Z, Zhang W, Zhou W, Yua L, and S. Lian S. Site-sensitive energy transfer modes in $Ca_3Al_2O_6:Ce^{3+}/Tb^{3+}/Mn^{2+}$ phosphors. Dalton Trans. 2014;43:18134–18145. doi:10.1039/c4dt01587h
91. Li K, Shang M, Zhang Y, Fan J, Lian H, Lin J. Photoluminescence properties of single-component white-emitting $Ca_9Bi(PO_4)_7:Ce^{3+},Tb^{3+},Mn^{2+}$ phosphors for UV LEDs. J Mater Chem C. 2015;3:7096–7104. doi:10.1039/c5tc00927h
92. Fan X, Si J, Xu M, Li G, Tang J, Cai G. Photoluminescence and energy transfer of efficient and thermally stable white-emitting $Ca_9La(PO_4)_7:Ce^{3+}$, Tb^{3+}, Mn^{2+} phosphors. Ceram Int. 2021;47:12056–12065. doi:10.1016/j.ceramint.2021.01.049
93. Wen D, Kato H, Kobayashi M, Yamamoto S, Mitsuishi M, Kakihana M. Site Occupancy and Luminescence Properties of $Ca_3Ln(AlO)_3(BO_3)_4:Ce^{3+}$, Tb^{3+}, Mn^{2+} (Ln = Y, Gd) Phosphors for White-LEDs. J Mater Chem C. 2017;5:4578–4583. doi:10.1039/C7TC00941K
94. Wang Z, Li P, Yang Z, Guo Q, Dong G. A white emitting phosphor $BaMg_2(PO_4)_2:Ce^{3+}$, Mn^{2+}, Tb^{3+}: Luminescence and energy transfer. Ceram Int. 2014;40:15283–15292. doi:10.1016/j.ceramint.2014.07.026
95. Huang C-H, Chen T-M. A Novel Single-Composition Trichromatic White-Light $Ca_3Y(GaO)_3(BO_3)_4:Ce^{3+},Mn^{2+},Tb^{3+}$ Phosphor for UV-Light Emitting Diodes. J Phys Chem C. 2011;115:2349–2355. doi:10.1021/jp107856d
96. Liu H, Luo Y, Mao Z, Liao L, Xia Z. A novel single-composition trichromatic white emitting $Sr_{3.5}Y_{6.5}O_2(PO_4)_{1.5}(SiO_4)_{4.5}$ $Ce^{3+}/Tb^{3+}/Mn^{2+}$ phosphor: synthesis, luminescent properties and applications for white LEDs. J Mater Chem C. 2014;2:1619–1627. doi:10.1039/c3tc32003k
97. Psuja P, Hreniak D, and Strek W. Rare-Earth Doped Nanocrystalline Phosphors for Field Emission Displays. J Nanomater. 2007;81350. doi:10.1155/2007/81350
98. Liao J, Zhou D, Yang B, Liu R, Zhang Q, Zhou Q. Sol-gel preparation and photoluminescence properties of $CaLa_2(MoO_4)_4:Eu^{3+}$ phosphors. J Lumin. 2013;134:533–538. doi:10.1016/j.jlumin.2012.07.033
99. Chen L, Chu C-I, Liu R-S. Improvement of emission efficiency and color rendering of high-power LED by controlling size of phosphor particles and utilization of different phosphors. Microelectron. Reliab. 2012;52:900–904. doi:10.1016/j.microrel.2011.07.058

 DOI: 10.15826/chimtech.2025.12.2.07